Ore Geology Reviews 101 (2018) 398–412

Contents lists available at ScienceDirect

Ore Geology Reviews

journal homepage: www.elsevier.com/locate/oregeorev

Characteristics of hydrothermal chlorite from the Niujuan Ag-Au-Pb-Zn deposit in the north margin of NCC and implications for exploration tools for ore deposits

Zhiqiang Wang[a,*], Bin Chen[b], Xiang Yan[a], Senwen Li[c]

[a] School of Resources and Environmental Engineering, Hefei University of Technology, Hefei 230009, Anhui, China
[b] Department of Earth and Space Sciences, Southern University of Science and Technology, Shenzhen 518055, Guangdong, China
[c] No. 3 Geological Party, Hebei Bureau of Geological Exploration, Zhangjiakou 075000, Hebei, China

ARTICLE INFO

Keywords:
Niujuan Ag-Au-Pb-Zn deposit
Chlorite geochemistry
Northern margin of NCC
LA-ICPMS

ABSTRACT

The Niujuan Ag-Au-Pb-Zn deposit is located in the northern Hebei Province of North China, which is hosted by Permian coarse-grained granite. The orebodies are controlled by a NE striking fault. Chloritization is the most extensive alteration with increasing alteration intensity from the distal to proximal end of the orebody. Chlorite and biotite from twenty-one altered samples from different depths of four drill holes were analyzed using electron microprobe (EMPA) and laser ablation inductively-coupled plasma mass spectrometry (LA-ICPMS). Empirical geothermometry shows that chlorite formed at 206–340 °C. Through comparing with compositions of unaltered biotite, two biotite converted to one chlorite (2Bt → 1Chl) is the main chloritization mechanism in weakly and moderately altered granites during the hydrothermal alteration in the Niujuan deposit. During the alteration, hydrothermal fluid mainly brought in Fe, Sr, Th, Pb and CO_2 and took out Mg, Ti, Si, F, K, Li, Zn, Sc, Ga, Co from the biotite, which was accompanied by the formation of quartz, rutile, calcite and fluorite during the chloritization. Chlorite in quartz-chlorite veins was precipitated directly from the hydrothermal fluids. Veined chlorite in intensely altered granites formed by the dissolution-transport-precipitation mechanism. Under the high fluid/rock conditions, veined chlorite has nearly the same compositions as chlorite in quartz-chlorite veins. According to the compositions of chlorite from intensely altered granites and quartz-chlorite veins, we infer that the hydrothermal fluid had low HFSEs and transition elements, such as Ti, Ga, Sc and V, and low fO_2. From weak to intense chloritization granites, FeO, Sr, Th and Pb contents of chlorite increase, while MgO, TiO_2, Li, Zn, Sc, Ga, V, Co and Nb contents decrease. The composition variations of chlorite are controlled by the composition of biotite, the compositions of fluids and the intensity of fluid-rock interaction during alteration. This indicates that the chemical variations of chlorite could be as a tool for mineral exploration in the moderate-low temperature Ag-Au-Pb-Zn deposit. Comparison with chlorite of different genesis shows that compositions of chlorite mainly differ in Mg, Fe and Al^{IV}, which are mainly controlled by the composition of host rocks and the formation temperature.

1. Introduction

Extensive alteration develops around hydrothermal deposits which are typically centered within an alteration halo that displays characteristic mineralogical and chemical zoning patterns (Lowell and Guilbert, 1970). The alteration patterns provide a key guide for a target area of exploration. Recent researches showed that compositions of alteration minerals are useful indicators for hydrothermal centers, especially in porphyry systems. EMPA and LA-ICPMS analyses of chlorite, epidote and alunite for porphyry systems revealed lateral and vertical composition variations from distal to proximal end of the orebody, which can be used as proximity indicator to the porphyry systems (Chang et al., 2011; Wilkinson et al., 2015; Xiao et al., 2017).

Chlorite, a hydrous phyllosilicate, is a common product of diagenesis, low-grade metamorphism and hydrothermal alteration and can form in a variety of rocks (De Caritat, 1993; Vidal et al., 2001; Yavuz et al., 2015). In most hydrothermal systems, chlorite is a major mineral occurring as an alteration of the surrounding rocks (Martinez-Serrano and Dubois, 1998). The structure of chlorite is characterized by regularly alternating tetrahedral-octahedral 2:1 sheets and interlayer

* Corresponding author.
E-mail address: wangzq@hfut.edu.cn (Z. Wang).

https://doi.org/10.1016/j.oregeorev.2018.08.003
Received 7 June 2017; Received in revised form 26 July 2018; Accepted 1 August 2018
Available online 02 August 2018
0169-1368/

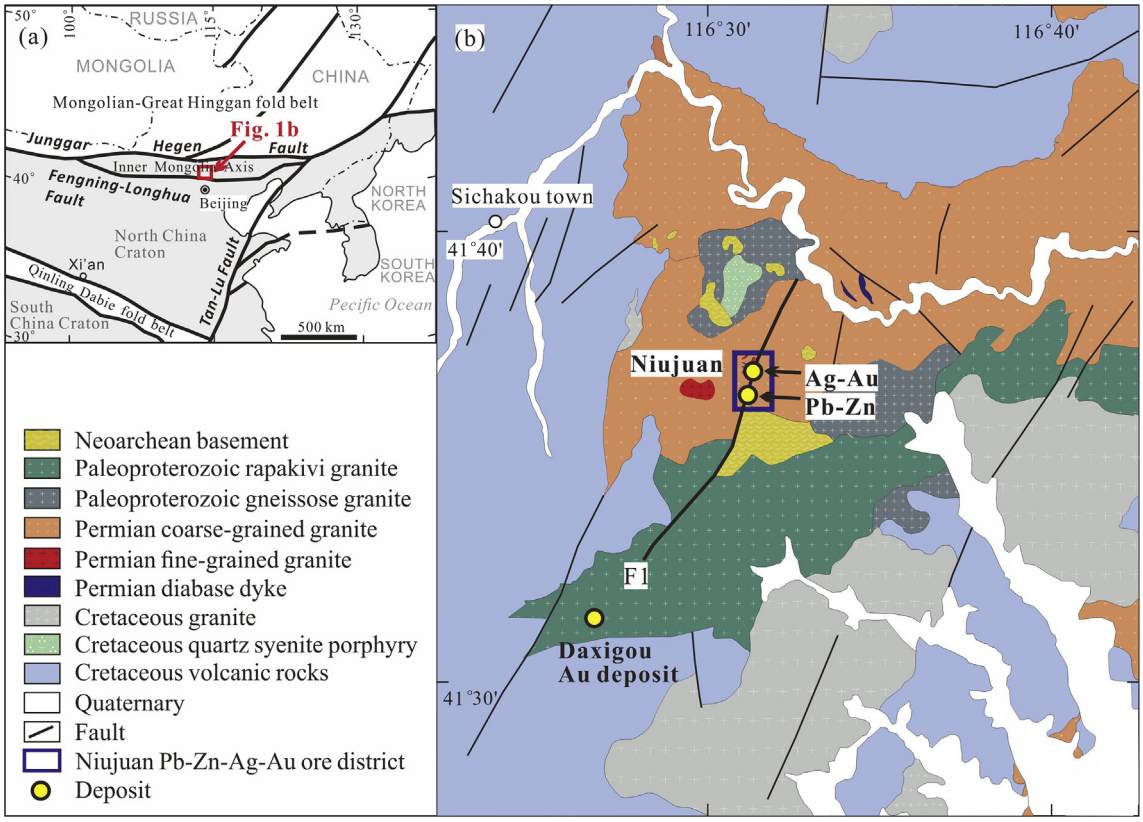

Fig. 1. (a) Main tectonic and structural elements of eastern China (modified after Hart et al., 2002). (b) Regional geological map of the Niujuan Pb-Zn-Ag-Au deposit, northern Hebei Province (modified after the geological map from the Yanshan Silver Corporation).

octahedral sheets. A general crystallochemical formulation of chlorite has been suggested to be: $(R_x^{2+}R_y^{3+}\square_{6-x-y})_6{}^{VI}(Si_{4-z}R_z^{3+})_4{}^{IV}O_{10}(OH)_8$, where $R_x^{2+} = Fe^{2+}$, Mg^{2+}, Mn^{2+}, Ni^{2+}, Co^{2+}, Zn^{2+} and Cu^{2+}; $R_y^{3+} = Al^{3+}$, Fe^{3+}, $\pm Cr^{3+}$, $\pm V^{3+}$; $\square$ = octahedral vacancy; $R_z^{3+} = Al^{3+}$, $\pm B^{3+}$, $\pm Fe^{3+}$ (Zane and Weiss, 1998). Chlorite has a wide range of non-stoichiometric compositional variations depending on bulk rock composition and physicochemical conditions prevalent at the formation (Inoue et al., 2010). Therefore, chemical compositions of chlorite are valuable to get information on the physicochemical conditions of the formation and on the exploration of deposits. The use of chlorite composition for estimating the formation temperature called as chlorite geothermometry has been used and discussed by many researchers (Cathelineau, 1988; Jowett, 1991; Zang and Fyfe, 1995; De Caritat, 1993; Xie et al., 1997; Vidal et al., 2006; Inoue et al., 2009; Bourdelle et al., 2013). Except for temperature, several other factors, including the bulk chemical composition of the host rock, the coexisting mineral assemblage, and the chlorite crystal structure, also influence the chemical variation of chlorite (Curtis, 1985; Bailey, 1988; Hillier and Velde, 1991; Xie et al., 1997). Chloritization of biotite via local dissolution-reprecipitation reactions is a common way to form chlorite, especially in intermediate-felsic igneous rocks. Several mechanisms have been proposed for the process of chloritization (Ferry, 1979; Veblen and Ferry, 1983; Parneix et al., 1985; Yuguchi et al., 2015), which is essential for recognizing the inflow and outflow components in the hydrothermal fluid. In addition, the compositions of chlorite in hydrothermal alteration zones change systematically with proximity to fluid pathways and hydrothermal veins and it can be used to trace the fluid compositions (Walshe 1986; Halter et al., 1998; Lanari et al., 2014). An important finding in exploration is that chlorite shows lateral and vertical composition variations from distal to proximal end of the orebody (Wilkinson et al., 2015; Xiao et al., 2017; Maydagán et al., 2018). However, since published data on the compositional variations of chlorite are mainly for high temperature porphyry ore-forming system, it is unclear whether these variations exist in moderate to low temperature deposits such as Pb-Zn or Ag-Au deposits. Besides, few studies have documented in detail the origin of chlorite in the alteration zone and its link with the mineralization. Chlorite of hydrothermal origin records the chemical characteristics of the hydrothermal fluid, which therefore provide an important clue to the mass transfer due to hydrothermal fluid advection in the pluton (Yuguchi et al., 2015), and are thus useful to determine alteration processes, fluid compositions and physicochemical conditions of mineralization (Bryndzia and scott, 1987a; Zang and Fyfe, 1995).

The Niujuan Ag-Au-Pb-Zn deposit is located in the northern Hebei province, North China. The orebody is hosted by Late Permian biotite monzogranite, which is controlled by the F1 fault (Nie et al., 2007). Chloritization is the most extensive alteration with the alteration intensity increasing from the distal to proximal end of the orebody (Li and Wang, 2002). The compositionally homogeneous host rock (granite) makes it possible to evaluate the influence of hydrothermal alteration on the chlorite composition, which is crucial to place a tight constraint on the nature of ore-forming fluids and their effects on chlorite composition. In this paper, we report EMPA and LA-ICPMS analyses of chlorite from drill holes in the Niujuan Ag-Au-Pb-Zn deposit, aiming to clarify the origin of chlorite and implications for the exploration tools.

2. Geological setting

Eastern Asia is mainly underlain by four ancient cratonic blocks: the Tarim, North China, South China and Siberian cratons, with each separated by intervening Phanerozoic orogenic belts (Hart et al., 2002). The orogenic belt between the North China and Siberian cratons is known as the Mongolian Great Hinggan fold belt, which is part of the Central Asian Orogenic Belt (Fig. 1a). A 1500 km-long EW-trending Au-Ag-Pb-Zn belt occurs at the northern margin of the North China Craton (NCC), which hosts a metal resource of ca. 900t Au and 20Mt Pb-Zn

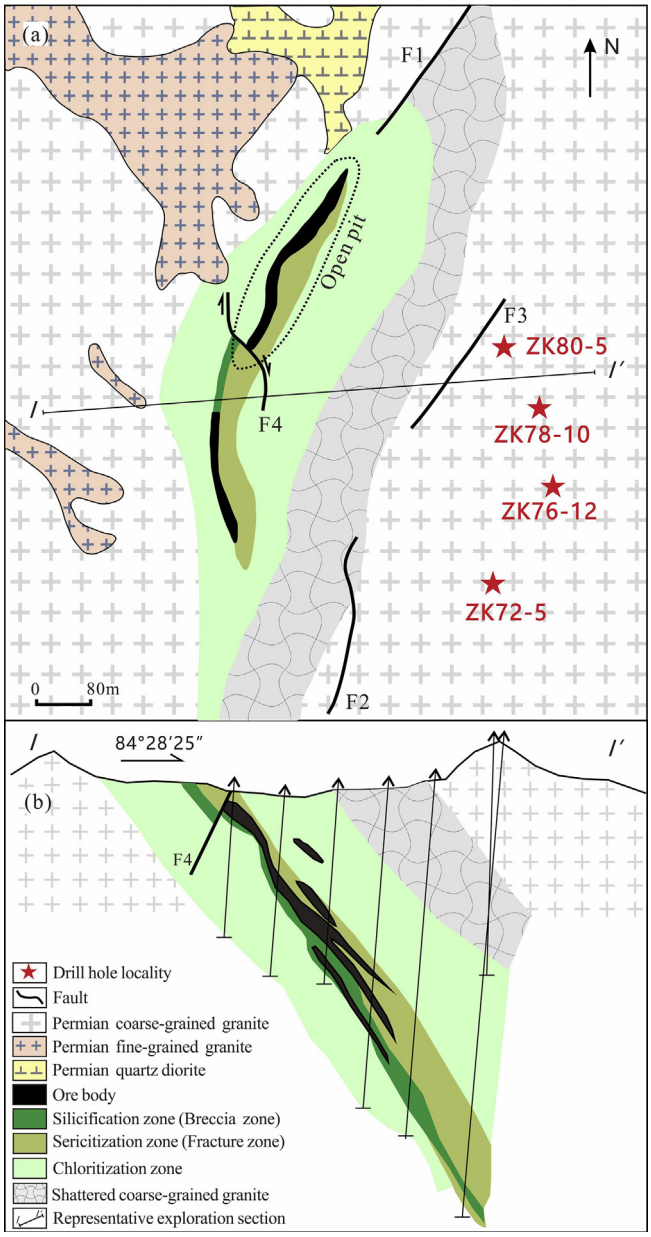

Fig. 2. (a) Simplified geological map of the Niujuan Pb-Zn-Ag-Au deposit (modified after Nie et al., 2007). (b) Geological cross section of the Niujuan deposit (modified after the geological map from the Yanshan Silver Corporation).

(Hart et al., 2002; Miller et al., 1998; Zhang and Zhu, 2016). Most polymetallic deposits lie in the so-called Inner Mongolia Axis, which is defined by the Junggar-Hegen fault zonein the north and the Fengning-Longhua fault in the south (Hart et al., 2002; Fig. 1a). The complex patterns of extensional and compressional structural features in the Inner Mongolia Axis are believed to have been caused by the collision between the NCC and Siberian craton and the subsequent circum-Pacific plate subduction beneath the East Asia (Davis et al., 1998). The eastern part of the NCC became tectonically active in the Late Mesozoic (known as the Yanshanian orogen), with large-scale magmatism, basin development, ductile deformation and movement on large-scale faults (Yang et al., 2003), which was associated with the westerly oblique subduction of the Izanagi plate. Intra-cratonic NNE-trending faults, represented by the Tan-Lu strike-slip fault and the Taihang fault, were related to this transpressive regime (Griffin et al., 1998).

Most deposits are hosted within Precambrian metamorphic rocks, but some deposits are hosted within Paleozoic or Mesozoic intrusions (Cook et al., 2009). The Precambrian metamorphic rocks consist of Neoarchean TTG gneiss and mafic rocks, Paleoproterozoic mafic *meta*-igneous rocks and *meta*-sedimentary rocks, and a small amount of Paleoproterozic carbonate rocks. The Precambrian metamorphic rocks are covered unconformably by the Middle Carboniferous to Triassic fluvial and deltaic sediments, and the Jurassic to Cretaceous and younger sediments and volcanic rocks.

Mafic to felsic granitoid batholiths, stocks and dykes are common throughout the northern margin of the NCC. These plutons were formed during the Proterozoic, Hercynian and Yanshanian orogens. The Hercynian orogen contains many Late Carboniferous to Early Permian diorite-quartz diorite-granodiorite plutons along the northern margin of the NCC (Zhang et al., 2009), which were intruded by the younger Yanshanian granitic intrusions. These Hercynian plutons show features of continental arc magmatism that could be associated with the southward subduction of the Paleo-Asian oceanic plate beneath the northern margin of the NCC during the Late Carboniferous to Early Permian period (Zhang and Zhao, 2013).

3. Ore deposit geology

The Niujuan Ag-Au-Pb-Zn deposit is located in the central part of the Inner Mongolia Axis. Twenty-six ore bodies were discovered in the Niujuan deposit, of which the No. 2 deposit is the main ore body. The northern part of the deposit is mainly composed of Ag and Au ore bodies. And the southern part is mainly composed of Pb-Zn ore bodies (Fig. 1b). Ore reserve in the Niujuan deposit is Ag 358t, Au 1.1t, Pb 85127t and Zn 105739t (Yanshan Silver Corporation). The Early Paleoproterozoic Hongqiyingzi group is the oldest lithological unit in this area and mainly comprises graphite biotite plagioclase gneiss, garnet biotite plagioclase gneiss, amphibolite and migmatic gneiss. The Hongqiyingzi group was covered by Cretaceous volcanic rocks which comprise andesite, dacite, rhyolite and rhyolitic tuff. The oldest intrusion in this area is the Late Paleoproterozoic mega-phenocryst coarse-grained biotite monzogranite. The Paleoproterozoic Hongqiyingzi group and mega-phenocryst monzogranite were intruded by Permian medium-coarse-grained biotite monzogranite, diabase dyke and fine-grained biotite monzogranite. The orebodies of the Niujuan are hosted in the Permian medium-coarse-grained biotite monzogranite (Fig. 2). The medium-coarse-grained monzogranite contains mainly K-feldspar (20–30%), plagioclase (35–55%), quartz (25–30%) and biotite (5–10%). Accessory minerals are zircon, apatite and magnetite (Fig. 3). The K-feldspar is commonly perthitic. Quartz and biotite are anhedral, being interstitial to K-feldspar and plagioclase, indicating they are the late-stage phases. The biotite was partially altered to chlorite because of the hydrothermal alteration. The fine-grained monzogranite occurs as a stock to the west of the deposit, intruding into the medium-coarse-grained monzogranite. The fine-grained monzogranite is composed of K-feldspar (45–55%), plagioclase (15–25%), quartz (30–35%) and biotite (3–5%), and accessory zircon, apatite, fluorite and allanite.

The orebodies are controlled by the F1 fault and hosted by the altered fractured granite (Fig. 2), occurring as "S" shape in the plane. The F1 fault zone is 8 km long and 10–34 m wide, striking 25–35° and dipping 52–65° SE (Wei, 2000), and is composed of the breccia and fault gouge. The breccia is the main ore-bearing rock unit, showing features of fragmentation, recrystallization and metasomatism textures. Fragments of the breccia include the medium-coarse-grained granite, early silicic rocks and detrital quartz and feldspar with irregular and angular shape (Fig. 3a). Matrix of the breccia is mainly the aphanitic quartz, part of which recrystallized to microcrystalline quartz. There are 40 orebodies along the ore zone. Single orebodies occur as lenses or dikes 40–450 m long and 0.73–8.1 m thick with 180–350 m down-dip extensions (Nie et al., 2007; Shen et al., 2012). Pyrite, galena and sphalerite are the most important metallic minerals, along with minor chalcopyrite, argentite, silver, gold, arsenopyrite, pyrrhotite,

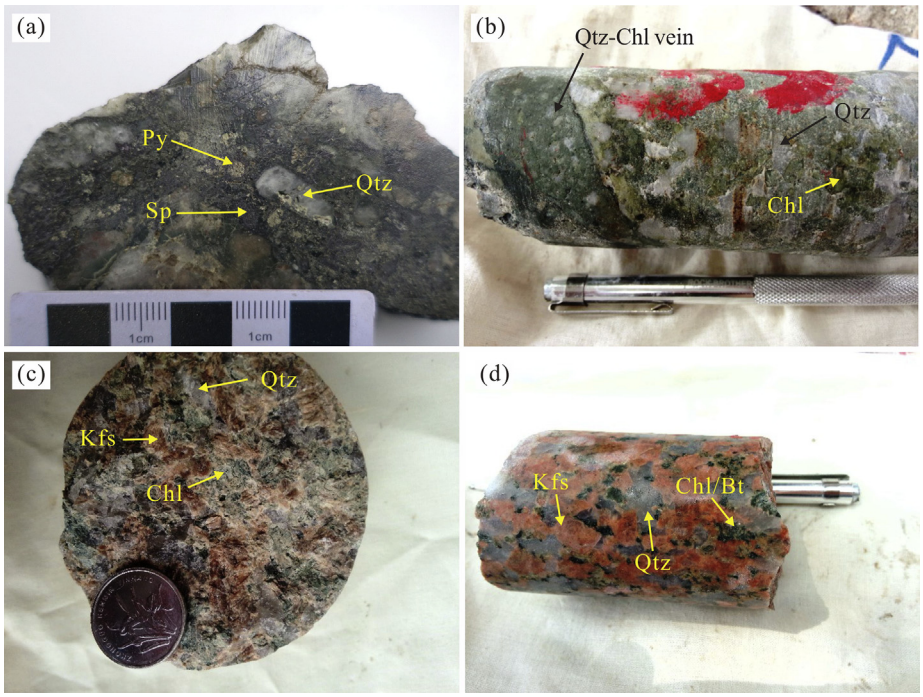

Fig. 3. Field photographs of ore and altered granites. (a) Silicic breccia from the open pit of Niujuan, with quartz fragment and pyrite and sphalerite mineralization, which is the main ore-bearing rock. (b) Intense chloritization granite (ZK80-5-15) showing dark green in color, which is cut by a quartz-chlorite vein. (c) Moderate chloritization granite (ZK72-5-46) showing light green in color. (d) Weak chloritization granite (ZK72-5-59) showing pinkish in color. Py, pyrite; Sp, sphalerite; Qtz, quartz; Chl, chlorite; Kfs, potash feldspar; Bt, biotite.

pyrargyrite, tetrahedrite, argentite and polybasite. Pyrite is the most widely distributed mineral present in all ore-forming stages and is the main host of Ag and Au. Besides, some Ag and Au are preserved in sphalerite, galena and arsenopyrite. Gangue minerals include quartz, mica, fluorite, feldspar, carbonates and clay minerals.

Silicification, sericitization and chloritization are the main alterations within the Niujuan deposit (Nie et al., 2007; Li et al., 2017; Fig. 2). The silicification zone is distributed in the core of the deposit, which constitutes the main orebody. The alteration minerals consist of aphanitic/microcrystalline quartz and minor sericite, hydromica and montmorillonite. The sericitization zone, extending wider than the silicification zone, formed in the breccia and the granite, which is composed of sericite with minor hydromica and aphanitic quartz. The granite around the orebodies shows extensive chlorite alteration, which is the most common alteration in the deposit. Chlorite is the main mineral in the chlorite alteration with minor calcite and pyrite.

Chloritization is the most extensive alteration type and shows different intensity from the proximal to distal end of the orebody. Generally, intense chloritization occurs in the proximal end of the ore body and weak chloritization occurs in the distal end (Fig. 4). Intense chloritization granite is dark green (Fig. 3b), in which chlorite is in the form of veinlets or lumps (Fig. 5). The associated minerals are quartz, fluorite, rutile and muscovite (Fig. 5). Moderate chloritization granite is light green to pinkish (Fig. 3c), in which biotite was totally converted to chlorite (Fig. 6a, b). Part of the chlorite is in the form of veinlets. Weak chloritization granite is pinkish (Fig. 3d), in which biotite was partly or totally converted to chlorite (Fig. 6c, d). The alteration is associated with the formation of rutile, quartz and potash feldspar in the chloritization part of biotite (Fig. 6e, f). In addition, quartz-chlorite veins (Fig. 3b) are widely distributed in the drill holes (Fig. 4). Quartz and chlorite are the predominant minerals with minor calcite, muscovite, potash feldspar, fluorite, magnetite (Fig. 7). Sphalerite, magnetite and pyrite appear in quartz-chlorite veins (Fig. 7c, d), indicating they formed during the mineralization.

4. Sampling and methods

Twenty-one granite samples with varied intensity of chloritization were collected from different depths of four drill holes in the Niujuan ore district. Sampling localities are shown in Fig. 4. Samples were prepared as thin sections for SEM backscattered electron imaging, electron microprobe analysis (EMPA) and laser ablation inductively-coupled-plasma spectrometry (LA-ICPMS).

Electron microprobe analyses of chlorite and biotite were carried out at the Ore Deposit and Exploration Centre (ODEC), Hefei University of Technology, China, using a JXA-8230 electron microprobe. Operating conditions were an acceleration voltage of 15 kV and a beam current of 1×10^{-8} A. The nominal spot diameter was 2 μm. The analytical accuracy is 1–5 percent.

Trace elements of chlorite and biotite were measured at the In situ Mineral Geochemistry Lab, Ore deposit and Exploration Centre (ODEC), Hefei University of Technology, China, using the Agilent 7900 Quadrupole ICP-MS connected with a Photon Machines Analyte HE 193-nm ArF Excimer Laser Ablation system. A squid signal smoothing device is included in this laser ablation system. Helium was applied as a carrier gas. Argon was used as the make-up gas and mixed with the carrier gas via a T-connector before entering the ICP. The in situ analyses were carried out on thin sections. Each analysis was performed by a uniform spot size diameter of 35 μm at 8 Hz with energy of ~2 J/cm^2 for 40 s after measuring the gas blank for 20 s. Standard reference materials GSE-1g, GSC-1g, BCR-2G and NIST 612 were used as external standards to plot calibration curve. The preferred values of element concentrations for the USGS reference glasses are from the GeoReM database (http://georem.mpch-mainz.gwdg.de/). Standard reference materials were run after each 10–15 unknowns; detection limits were calculated for each element in each spot analysis. The off-line data processing was performed using a program called ICPMSDataCal (Liu et al., 2008). Si concentrations obtained by EPMA were used as internal standard. Each spectrum was inspected in detail. Segments of the spectrum related to inclusions were removed. Analytical error for mineral for most major and trace elements are 5% and 10%, respectively.

5. Results

Microprobe analyses and trace-element compositions of chlorite are given in supplementary table 1 and Supplementary table 2, respectively. To avoid contamination by other phyllosilicate minerals, chlorite analyses with more than 0.5% ($Na_2O + K_2O + CaO$) were rejected

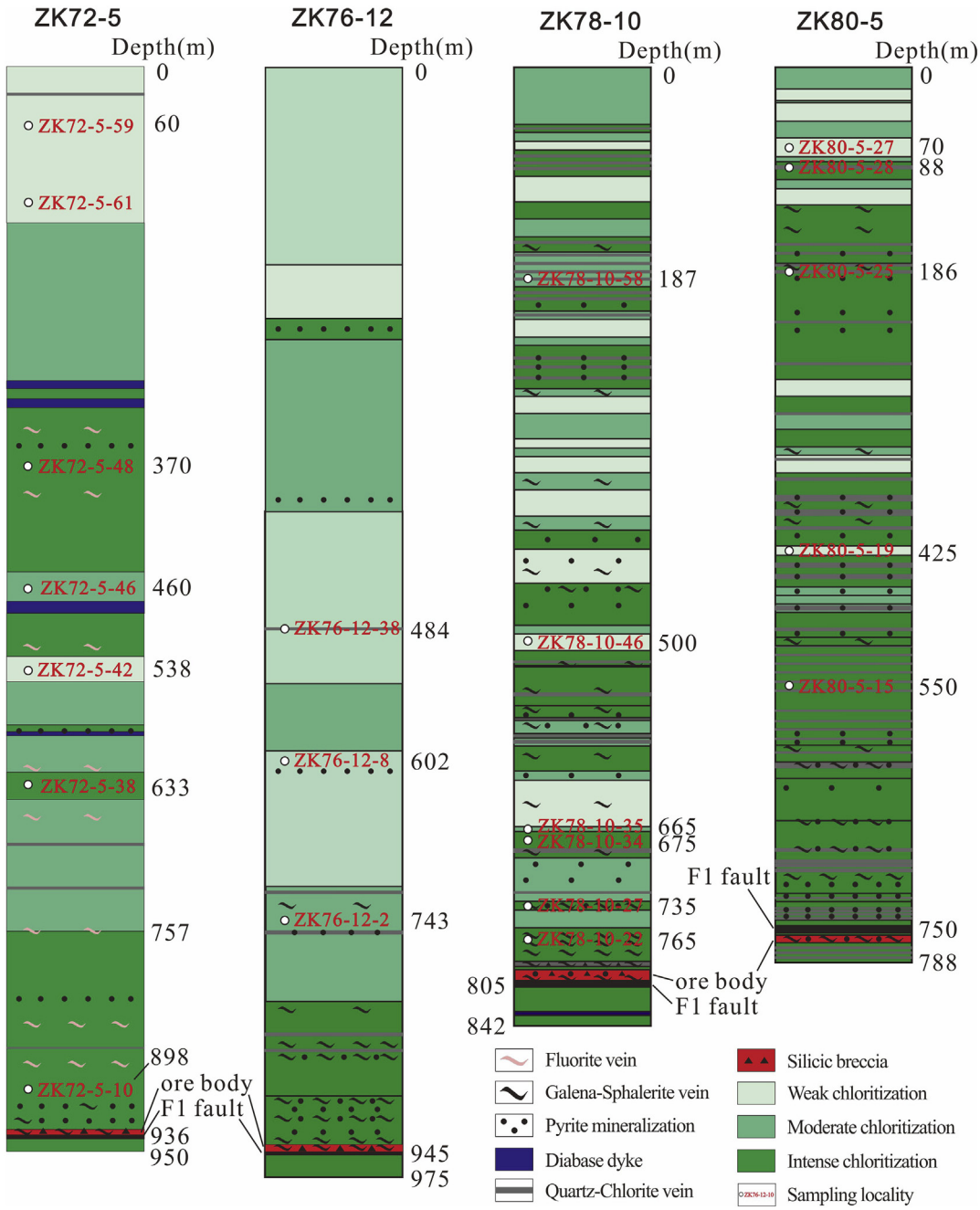

Fig. 4. Geological section map of four drilling holes of the Niujuan deposit, showing the sampling localities.

(Vidal and Parra, 2000). In LA-ICPMS analyses, for the large spot size, part of data were filtered by the standard of $Na_2O + K_2O + CaO < 1\%$. Most of the data (> 80%) have a $Na_2O + K_2O + CaO$ content less than 0.5%. Because of the widely distributed mineral inclusions of titanium dioxide (Fig. 6b, e, f), we use the Ti contents analyzed by EMPA with 2 μm spot size rather than by LA-ICPMS with 35 μm spot size.

Chlorite at Niujuan has high FeO content (32.19–41.85%) and relatively low MgO (2.32–8.30%) and SiO_2 (22.26–28.36%) contents. In the classification of Foster (1962), chlorite corresponds mainly to chamosite and thuringite, with Fe/(Fe + Mg + Mn) = 0.68–0.90 (Fig. 8a). The FeO content increases, and MgO and SiO_2 contents decrease from chlorite in the weakly altered samples to those in the intensely altered samples (Fig. 9). Chlorite from quartz-chlorite veins has similar compositions to chlorite in intensely altered samples (Fig. 9). Small variations are observed for Al_2O_3 (16.61–21.39%) in different samples (Fig. 9d). The contents of F are various and indistinguishable between different intensity of chloritized samples (Supplementary Table 1). Similarly, chlorite from variably altered zones have distinct trace elements. Chlorite from the intensely altered samples and quartz-chlorite veins has lower Li (175–550 ppm), Zn (218–1369 ppm), Sc (0–11.84 ppm), Ga (27.8–73.6 ppm), Co (16.2–37.2 ppm) and Nb (0.15–4.58 ppm, except for the abnormally high values of sample ZK72-5-10) contents than those from the weakly altered samples (Fig. 10), but have high Sr (5.0–120.9 ppm), Th (0.22–5.07 ppm) and Pb (0.26–12.98 ppm) contents (Fig. 10a–c).

Chlorite shows a wide range of compositional variations due probably to the three main substitutions: $Mg^{2+} \leftrightarrow Fe^{2+}$, Tschermark $Si + (Mg^{2+}, Fe^{2+}) \leftrightarrow Al^{IV} + Al^{VI}$ and di-trioctahedral $\square + 2Al^{VI} \leftrightarrow 3(Mg^{2+}, Fe^{2+})$ where $\square$ = octahedral vacancy, controlled by fluid

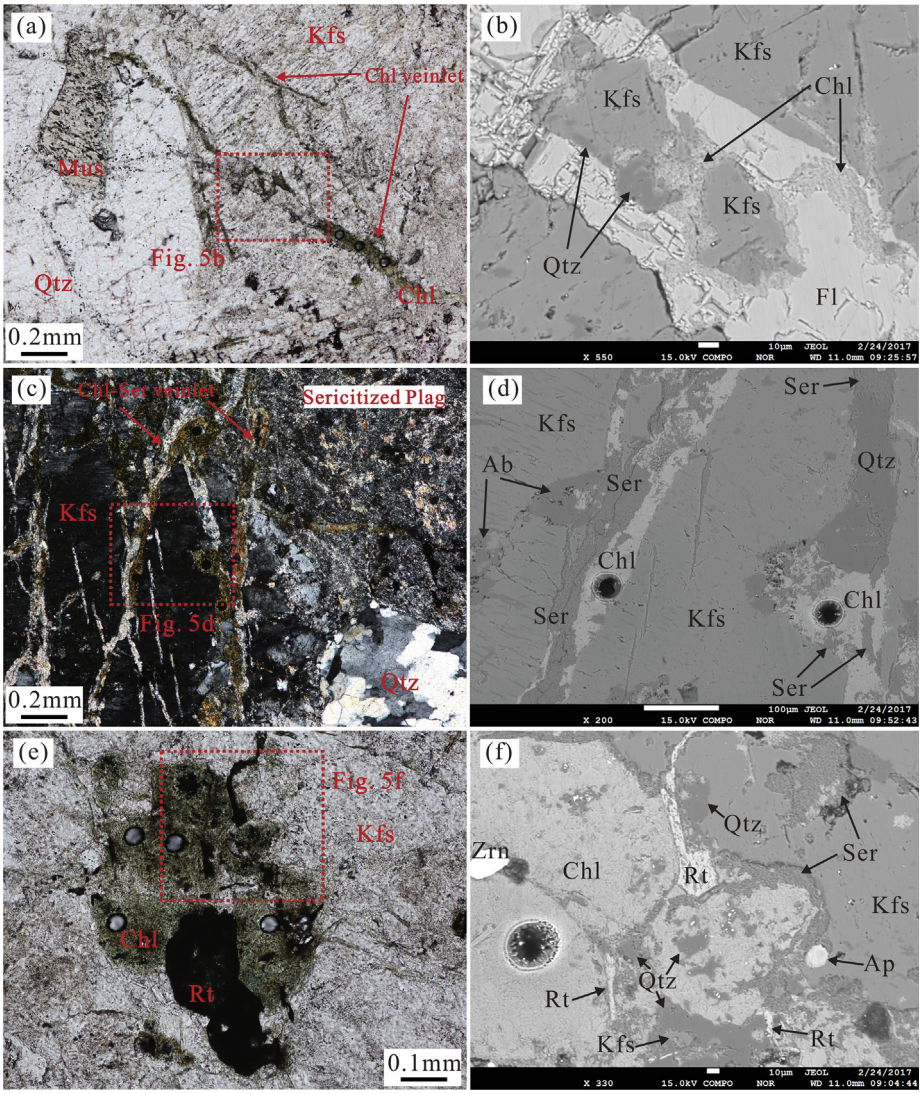

Fig. 5. Microphotographs and backscattered electron (BSE) images of chlorite from the intense chloritization granites. (a, b) Chlorite in the form of veinlet from sample ZK72-5-38, in which chlorite coexists with potash feldspar, quartz and fluorite. (c, d) Chlorite in the form of veinlet from sample ZK72-5-10, in which chlorite coexists with sericite and quartz. (e, f) Chlorite in the form of lump from sample ZK72-5-10. Sericite is present in the edge of chlorte. Chl, chlorite; Qtz, quartz; Fl, fluorite; Rt, rutile; Kfs, potash feldspar; Zrn, zircon; Ap, apatite; Ser, sericite; Mus, muscovite; Plag, plagioclase; Ab, albite.

physicochemical properties and the bulk rock composition (Bourdelle et al., 2013; Yavuz et al., 2015). Chlorite from weak and intense chloritization samples has different cation substitutions. The Mg → Fe substitution dominates the octahedral substitution in weak chloritization samples, as revealed by the negative relationships in Fig. 11a. Al^{IV} enters chlorite through the Tschermark substitution. Part of the value of Al^{VI} is smaller than the value of Al^{IV} (Fig. 11b), indicating that additional octahedral R^{3+}, such as Fe^{3+}, may have replaced Al^{VI}. Most chlorite in intensely altered and quartz-chlorite samples has higher Fe and Al^{VI} than weakly altered samples (Fig. 11b, c). In addition, most Al^{VI} values are greater than Al^{IV} in these samples (Fig. 11b). This suggests that the di-trioctahedral substitution, $3(Fe^{2+}, Mg^{2+}) \rightarrow \square + 2Al^{VI}$, prevails in intensely altered and quartz-chlorite samples.

Microprobe analyses and trace-elements of biotite are given in Supplementary table 3 and Supplementary table 4, respectively. Biotite from the Niujuan ore deposit are characterized by relatively Fe-rich and Mg-poor compositions, close to annite end member in the diagram of mica classification (Rieder et al., 1998), showing lower Fe/(Fe + Mg + Mn) ratios than chlorite (Fig. 8b). Biotite has relatively uniform compositions, with SiO_2 = 36.09–37.49%, MgO = 5.56–6.43%, TiO_2 = 2.59–3.47%, FeO = 24.78–27.28% and Al_2O_3 = 12.26–13.32% (Fig. 9). In trace elements, biotite shows high Li (490–898 ppm), Sc (77.5–106 ppm), V (79–121.7 ppm) and Nb (147–323 ppm) contents, but low Sr (0.406–6.61 ppm), Th (0–0.36 ppm) and Pb (2.36–19.2 ppm) contents (Fig. 10).

6. Discussion

6.1. Chlorite geothermometry

Chlorite shows large non-stoichiometric compositional variations influenced by the bulk rock composition and physicochemical conditions during the process of chloritization. Therefore, compositional variations of chlorite are valuable to acquire the physicochemical conditions. Three approaches of chlorite geothermometry have been proposed: (1) polytype geothermometry based on the structural changes which may be partly temperature-dependent (Hayes, 1970; Walker, 1993); (2) empirical calibrations between the Al^{IV} occupancy and/or the octahedral vacancy and the measured temperature in geothermal systems and homogenization temperatures of fluid inclusions in geothermal systems (Cathelineau and Nieva, 1985; Cathelineau, 1988; Hillier and Velde, 1991); and (3) thermodynamic calculation

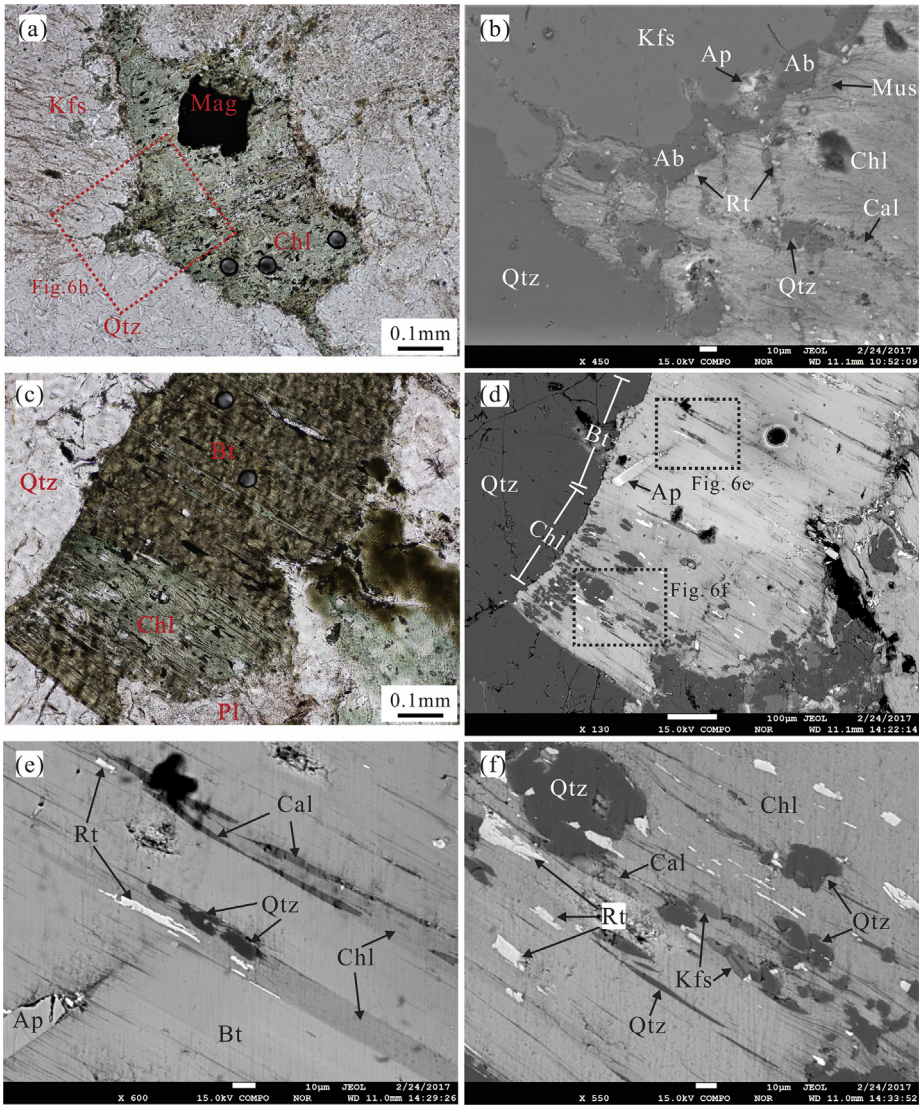

Fig. 6. Microphotographs and backscattered electron (BSE) images of chlorite from the moderate-weak chloritization granites. (a, b) Totally chloritized biotite from sample ZK72-5-46. (c–f) Partially chloritized biotite from sample ZK72-5-59. Chlorite, quartz, rutile, calcite and potassium feldspar are preferentially along cleavage planes in biotite. Bt, biotite; Chl, chlorite; Qtz, quartz; Fl, fluorite; Rt, rutile; Kfs, potash feldspar; Cal, calcite; Ap, apatite; Ab, albite; Mus, muscovite; Mag, magnetite.

based upon the activities of end-member components of chlorite, considering the tschermakite and di-tri substitutions as functions of formation temperature (Walshe, 1986; Vidal et al., 2001; Inoue et al., 2009). Among these approaches, the Al^{IV} geothermometry was widely used in the past decades. McDowell and Elders (1980) and Jahren and Aagaard (1989) reported that Al^{IV} increases with increasing chlorite formation temperature. The Al^{IV} geothermometry was first proposed by Cathelineau and Nieva (1985) and modified by Cathelineau (1988), which is an empirical calibration based on a linear increase of Al^{IV} content with chlorite formation temperature from the Los Azufres and Salton Sea geothermal system. Several authors argued that the Al^{IV} content in chlorite also depends on the bulk-rock composition, generally showing a positive correlation with Fe/(Fe + Mg) ratios (De Caritat, 1993; Jiang and Peacor, 1994). Considering the effect of the bulk-rock composition, several tentative corrections based on the Fe/(Fe + Mg) ratio were introduced in the empirical equations (Kranidiotis and McLean, 1987; Jowett, 1991; Zang and Fyfe, 1995; Xie et al., 1997). We calculated the temperatures using different empirical equations (Fig. 12). The thermometers of Cathelineau and Nieva (1985) yield comparable calculated T with a maximum temperature of 206–340 °C, which are consistent with the homogeneous temperatures of fluid inclusion in quartz associated with mineralization from the Niujuan deposit (230–310 °C; Chen et al., 2007). The thermometers with significant Fe/(Fe + Mg) correction on the calculated temperature (Hillier and Velde, 1991; Zang and Fyfe, 1995; Xie et al., 1997) give results significantly lower or higher than the homogeneous temperatures of fluid inclusions (Fig. 12), which indicates that the correction of Fe/(Fe + Mg) may not be necessary in our samples. Therefore, we believe that the temperatures calculated by the method of Cathelineau and Nieva (1985) represent the temperatures of chlorite formation. From the results, different chloritization intensity samples show the similar range of formation temperature, suggesting that they formed in the same hydrothermal event.

6.2. Chloritization process of biotite

The textures show that chlorite in weakly and moderately altered samples formed by chloritization of biotite (Fig. 6a, c). Biotite chloritization occurs under a wide temperature range below about 400 °C (De Caritat, 1993). The chloritized biotite is coupled with various secondary phases, such as muscovite, corrensite, smectite, calcite, epidotes, Ti-oxides and sulfides (Parneix et al., 1985; Yuguchi et al., 2015).

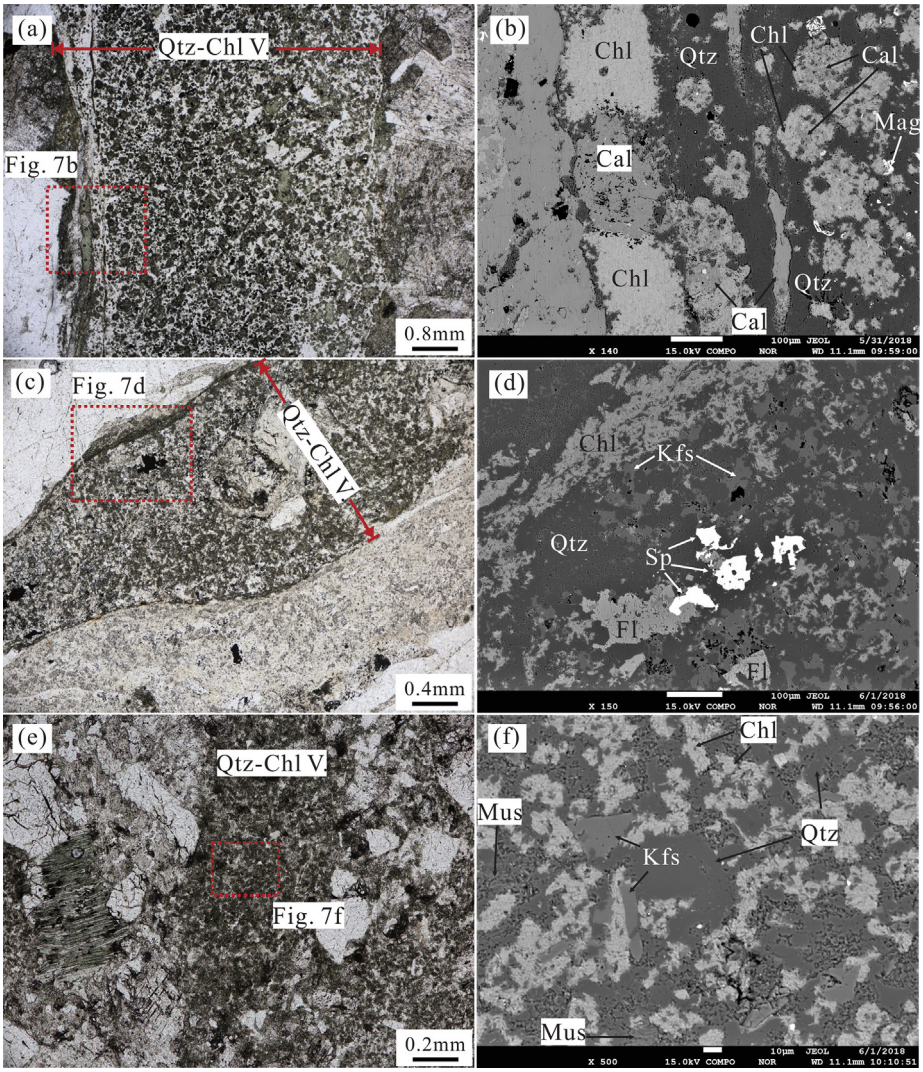

Fig. 7. Microphotographs and backscattered electron (BSE) images of chlorite from quartz-chlorite veins. (a and b) are from sample ZK76-12-38. (c and d) are from sample ZK78-10-22. (e and f) are from sample ZK78-10-58. Chl, chlorite; Qtz, quartz; Cal, calcite; Mag, magnetite; Fl, fluorite; Kfs, potash feldspar; Mus, muscovite; Sp, sphalerite; V., vein.

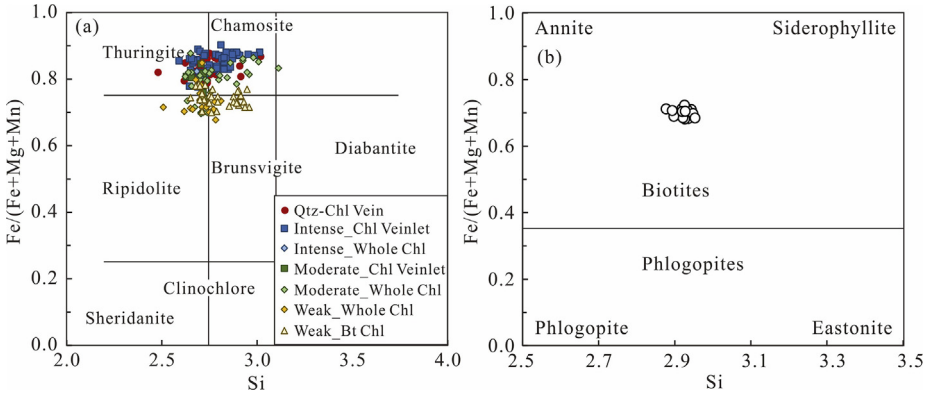

Fig. 8. (a) Classification diagram of chlorite from the Niujuan deposit (after Foster, 1962). (b) Classification diagram of unaltered biotite from the Niujuan deposit (after Rieder et al., 1998).

Biotite is altered to chlorite through mechanisms as below: (1) layer-by-layer replacement which is characterized by metasomatic textures of chlorite, and (2) dissolution-transport-precipitation process which results in the formation of relatively coarse-grained aggregates of chlorite or veined chlorite along the fissure (Jiang and Peacor, 1994). Chlorite partially or totally replacing biotite, but preserving the crystal form of biotite, in weakly and moderately altered samples, probably formed as a result of layer-by-layer replacement mechanism. The conversion of biotite to chlorite, quartz, rutile, calcite and potassium feldspar takes place preferentially along cleavage planes in biotite (Fig. 6e, f).

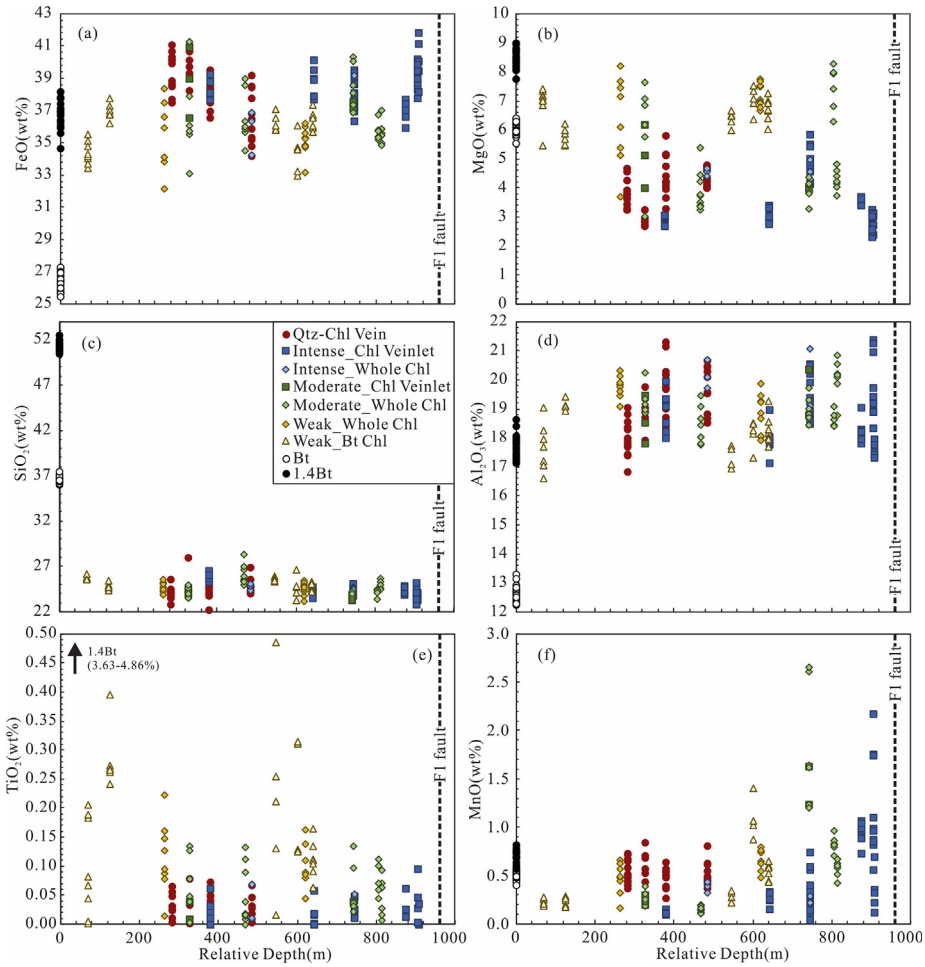

Fig. 9. Plots of major elements concentrations in chlorite as a function of depth. To eliminate the influence of various F1 fault depths of different drill holes, Relative sample depth is used in this figure, which is sample depth normalized to the deepest F1 fault of 945 m. F1 fault represents the center of hydrothermal fluid and mineralization.

Two different chloritization mechanisms are responsible for forming a single layer of chlorite in biotite. One is 1Bt → 1Chl, meaning that one biotite layer is transformed into one chlorite layer, forming a brucite-like layer into the interlayer region between two TOT biotite layers. This mechanism requires inflow of substantial materials (including metallic ions, like Al, Fe and Mg, and H_2O/H^+) and outflow of interlayer potassium and results in an increase in volume (Veblen and Ferry, 1983; Yuguchi et al., 2015). The other one is 2Bt → 1Chl, meaning that two biotite layers becomes one chlorite layer, forming a brucite-like layer by removal of the tetrahedral sheets of one TOT biotite layer. This mechanism requires inflow of H_2O/H^+ and outflow material (including tetrahedral components, like Si and Al, octahedral components, like Ti, Fe and Mg, and interlayer potassium) from the crystal and results in a decrease in volume (Veblen and Ferry, 1983; Yuguchi et al., 2015). In order to disclose the chlorization mechanisms and the inflow and outflow of chemical components during chloritization in the Niujuan samples, we calculate the simulated compositions of chlorite formed by the above two chloritization mechanisms (Supplementary Table 5), respectively, and make a comparison with the analyzed biotite and chlorite compositions (Fig. 13). We suggest that the mechanism 2Bt → 1Chl is the main alteration mechanism for reasons as below. Firstly, the compositions of chlorite by mechanism 2Bt → 1Chl have Fe, Si and Al^{IV} similar to that from the weak chloritization samples (Fig. 13a, b, d). While the compositions of chlorite by mechanism 1Bt → 1Chl show significantly lower Fe and Mg than that from the weak chloritization samples (Fig. 13a). This means that large amounts of Fe and Mg need to be introduced into the process of chloritization, but the biotite (1Bt → 1Chl) could not provide extra Fe and Mg. Moreover, no other mafic minerals in the granite of the Niujuan ore deposit can provide such large amounts of Fe and Mg components for the chloritization. Secondly, petrological data show that abundant quartz formed during the process of chloritization of biotite (Fig. 5d, f, Fig. 6e, f), suggesting outflow of considerable amounts of Si during the chloritzation, which is the case for the mechanism 2Bt → 1Chl rather than for 1Bt → 1Chl (Fig. 13b). In addition, no deformation signature in the chloritized biotite rules out the possibility of the mechanism 1Bt → 1Chl. Volume decrease caused by 2Bt → 1Chl is compensated by the newly formed quartz. Thirdly, two biotite layers have the same Al as one chlorite layer analyzed (Fig. 13b). This suggests Al is conserved in the biotite-chlorite system during chloritization, which is consistent with previous studies that Al is less mobile in fluid (Shriver and Maclean, 1993). But in the case of 1Bt → 1Chl, a lot of Al is required to be introduced into chlorite from other Al-bearing minerals. Although Al could be released from surrounding feldspar during sericitization and part of which could be introduced to biotite-chlorite system (Morad et al., 2009), the mechanism 2Bt → 1Chl seems more reasonable than 1Bt → 1Chl.

In the process of chloritization (2Bt → 1Chl), Al^{IV} removed from the tetrahedral sites of biotite is not carried away by the hydrothermal fluid but occupies the octahedral sites of new chlorite, which agrees with the homogeneity of Al content in chlorite (Fig. 13b–d). Large amounts of Al^{VI} in chlorite, much more than biotite, are required for (1) electrostatic bonding between the hydroxide interlayer and the TOT layer and (2) neutralization of negative charge on the tetrahedral sheets (Ryan and Reynolds, 1996). The considerable amounts of Al occupying the

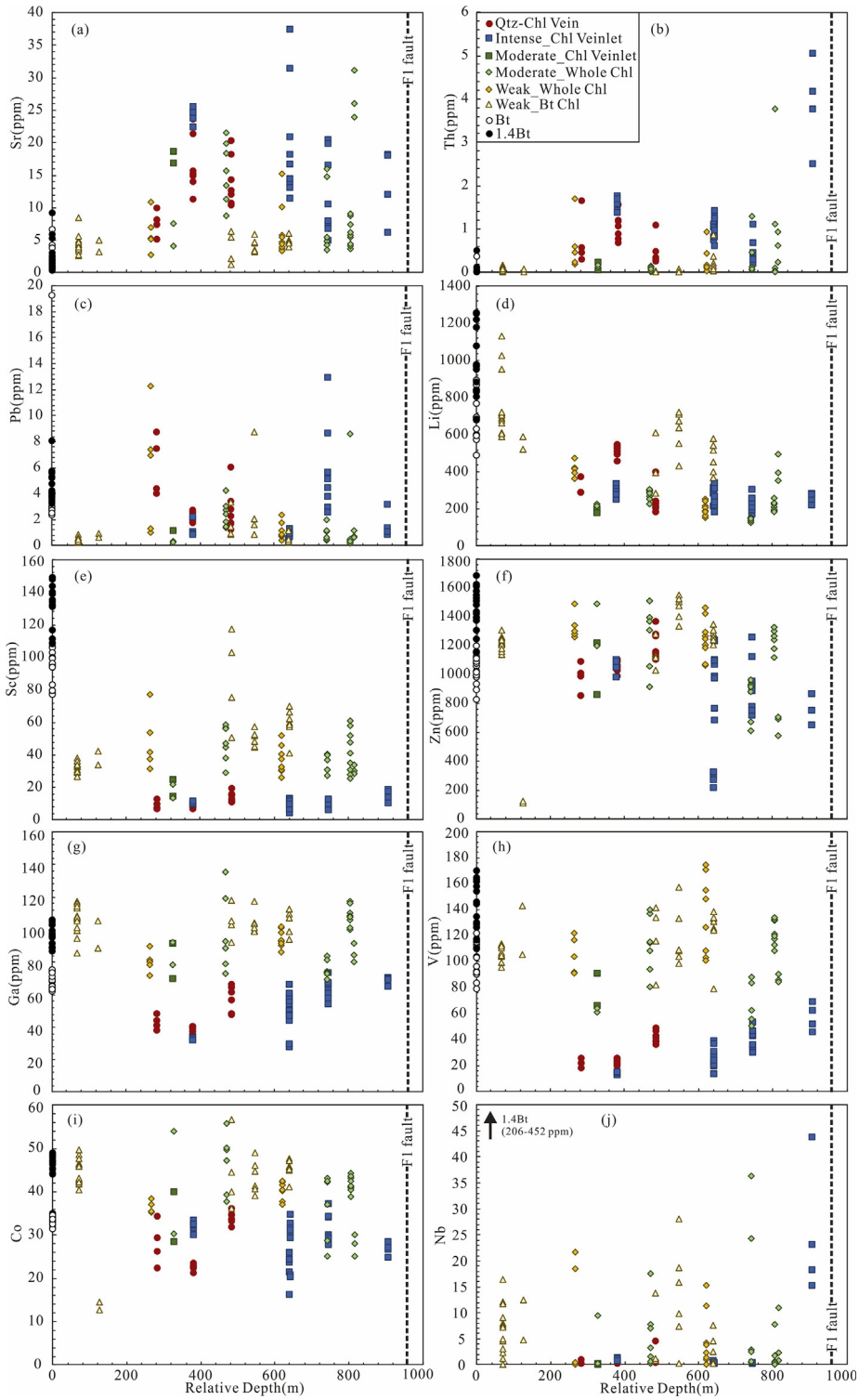

Fig. 10. Plots of trace elements concentrations in chlorite as a function of depth. To eliminate the influence of various F1 fault depths of different drill holes, Relative sample depth is used in this figure, which is sample depth normalized to the deepest F1 fault of 945 m. F1 fault represents the center of hydrothermal fluid and mineralization.

octahedral sites exclude Ti from both octahedral sheets in chlorite (Fig. 9e). The released Ti formed platy rutile nanoparticles between biotite/chlorite layers (Fig. 5f, 6f). Titanium occurring as oxides (rutile) rather than in silicates (e.g. titanite) may have been attributed to the high oxygen fugacity, temperatures and the effect of CO_2 (Jiang and Peacor, 1994; Ryan and Reynolds, 1997; Papoulis et al., 2009). The presence of calcite in alteration minerals (Fig. 6b, e, f) indicates that CO_2 was brought in by the hydrothermal fluid, which is supported by the abundance of CO_2-rich fluid inclusions in the orebody (Chen et al., 2007). Part of Mn and most K and F of biotite were released during chloritization. Fluorine reacts with Ca from break-down of plagioclase, forming fluorite in the altered granites (Fig. 5b). Potassium was mostly taken away by the hydrothermal fluids, some may be hosted in the newly formed potassium feldspar (Fig. 5b, Fig. 6f; Chayes, 1955;

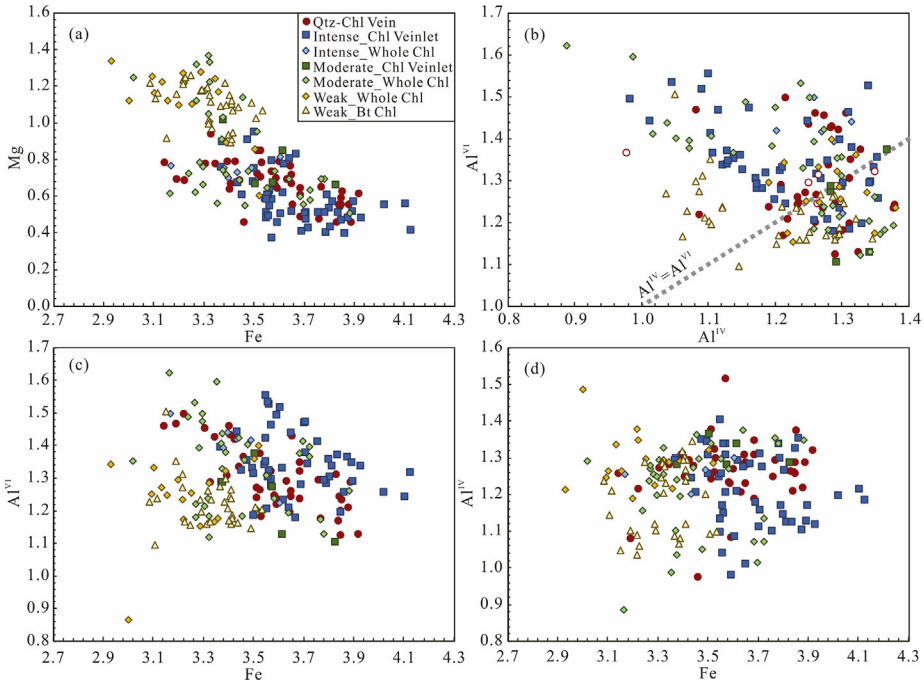

Fig. 11. Scatter diagrams of major cations (atoms pfu). (a) Fe and Mg have a negative relationship in moderate-low chloritization granites, and have a flat relationship in intense chloritization granites. (b) The data with Al^{IV} greater than Al^{VI} indicate that additional octahedral R^{3+}, such as Fe^{3+}, may have replaced Al^{VI}. The data with Al^{IV} smaller than Al^{VI} suggest the octahedral R^{3+} in excess of Al^{IV} have replaced R^{2+} in a 2:3 ratio. (c) Intensely altered granites and quartz-chlorite veins show relatively higher Al^{VI} content than weakly altered samples. (d) There is no obvious relationship between Fe and Al^{IV}.

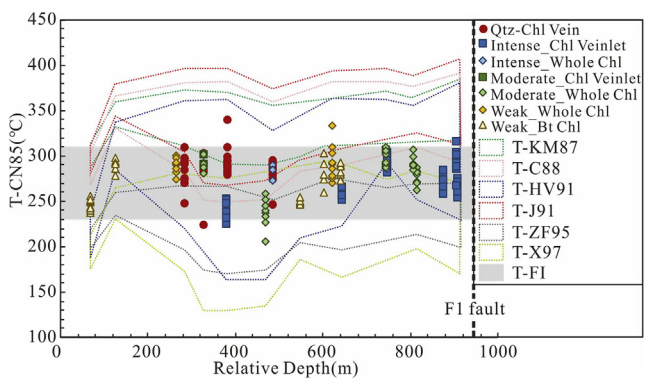

Fig. 12. Calculated temperature of chlorite formation using method of Cathelineau and Nieva (1985), compared to other chlorite geothermometers and homogenization temperature of fluid inclusion in the Niujuan deposit. T-CN85, from Cathelineau and Nieva (1985); T-KM87, from Kranidiotis and McLean (1987); T-C88, from Cathelineau (1988). T-J91, from Jowett (1991); T-HV91, from Hillier and Velde (1991); T-ZF95, from Zang and Fyfe (1995); T-X97, from Xie et al. (1997); T-Fl, homogenization temperature of fluid inclusion in the Niujuan deposit (Chen et al., 2007).

Eggleton and Banfield, 1985; Yuguchi et al., 2015). In some cases, potassium was preserved by the newly formed muscovite (Fig. 5c, e).

As discussed above, Al_2O_3 content should keep constant during the alteration from biotite to chlorite during weak chloritization. Hence, a correction coefficient could be defined by average Al_2O_3 content of chlorite divided by average Al_2O_3 content of biotite, which is about 1.4. This means that the reaction of 2Bt → 1Chl in stoichiometry is equivalent to 1.4Bt → 1Chl in mass fraction. When we discuss the mass transfer of chemical components in the biotite-chlorite reaction, we compare data between 1.4Bt and 1Chl in the mass fraction. Nearly all Fe, Al and Mn of biotite entered new formed chlorite during alteration (Fig. 9a, d, f). Little Mg and abundant Si and Ti were lost during chloritization (Fig. 9b, c, e). A small amount of Li and Sc were also lost during chloritization (Fig. 10d, e), indicating that Li and Sc were partially mobile in fluid. While, weak and moderate chloritization samples have similar contents of Zn, Ga, V and Co with 1.4Bt (Fig. 10f–i), indicating these elements retained in chlorite during chloritization. The different variations of trace elements in chlorite may result from the different element mobility in hydrothermal fluid. We can conclude that compositions of chlorite in weak and moderate chloritization samples were mainly controlled by the compositions of biotite and the element mobility in hydrothermal fluid.

6.3. Formation of veined chlorite and implications for the hydrothermal fluid

For chlorite in quartz-chlorite veins (Fig. 7), we believe that it was not formed by the alteration of biotite, but was precipitated directly from the hydrothermal fluids (cf. Beaufort et al., 2015). This suggests that the chlorite chemistry formed as a result of open-space precipitation from a fluid, which is consistent with our data that chlorite in quartz-chlorite veins shows significantly lower fluid immobile elements, such as Ti, Nb, Sc, Ga, V, Co and Ni, contents than altered chlorite (Figs. 9, 10). On the contrary, fluid mobile elements, such as Th, Pb and Sr, are relatively enriched in veined chlorite (Fig. 10). Sphalerite, magnetite and pyrite are present in quartz-chlorite veins (Fig. 7b, d), suggesting that the veins were formed during the mineralization. The ore-forming fluid should have high Zn, Pb, Co, V and Ni contents because of abundant sulfide minerals, which are significant hosts of Zn, Pb, Co, V and Ni (Brzozowski et al., 2018), in the orebody. However, these elements in chlorite from quartz-chlorite veins are depleted except for the slightly Pb enrichment (Fig. 10). We infer that these elements were sequestered by the precipitation of sulfide minerals near the F1 fault. Subsequently, quartz-chlorite veins formed from the upward migration of residual ore-forming fluid.

Chlorite in veinlets from intensely altered samples should be formed by the dissolution-transport-precipitation mechanism, indicating a strong hydrothermal activity and high water/rock ratios conditions. Different from weakly and moderately altered samples, in which Mg → Fe substitution dominates the octahedral substitution, the di-trioctahedral substitution, $3(Fe^{2+}, Mg^{2+}) \rightarrow \square + 2Al^{VI}$, controls the chemical variations of chlorite from intensely altered samples (Fig. 11). The compositional differences presumably reflect different modes of chlorite growth. In intensely altered samples, some biotite was altered to muscovite which connected with the veined chlorite (Fig. 5a). The veined chlorite distributes along the fractures in these samples. This

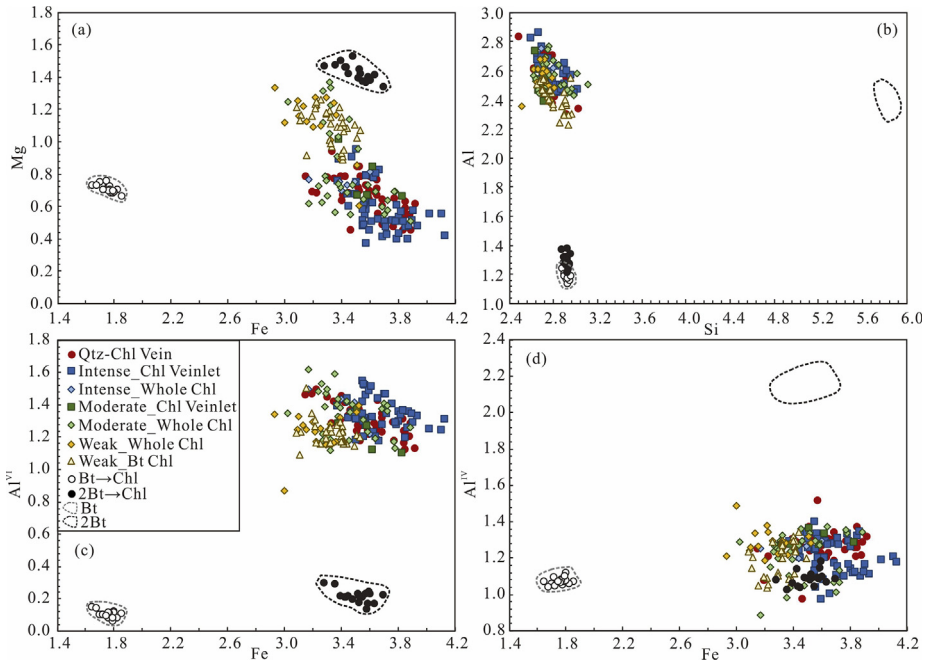

Fig. 13. Diagrams of major cations (atoms pfu) in chlorite. In order to clarify the chloritization mechanism in the Niujuan samples and the compositions brought in by the hydrothermal fluid, composition of chlorite calculated by the mechanism 1Bt → 1Chl and 2Bt → 1Chl and composition of biotite are added to make comparisons.

texture implies that the Fe and Mg migrated with fluid from biotite to veined chlorite. Al in biotite may be kept in muscovite, hence Al in veined chlorite probably came from the hydrothermal fluid or the surrounding plagioclase. The view that Al came from the surrounding plagioclase is supported by the presence of chlorite-sericite veinlets, which are connected with the intensely sericitized plagioclase (Fig. 5c, d). Abundant Al was released during the sericitization may account for the slightly high Al content of chlorite from intensely altered granites (Fig. 13b). Chlorite in veinlets in intensely altered samples has the nearly same compositions as in quartz-chlorite veins, such as low Mg, Ti, Sc, Ga and V contents, and high Fe, Sr and Th contents. We propose that when hydrothermal fluid passed through the host rock in high intensity, Mg and Fe were removed from biotite and participated in the neighboring fractures. Because most high field strength elements and transition elements were locked in the altered assemblage, such as muscovite + rutile + Fe-Oxide, veined chlorite was depleted in these elements and mainly reflected the composition of the fluid.

The Fe/(Fe + Mg) ratios in chlorite increase from the weakly altered granites to intensely altered granites (Fig. 8). Experimental studies and related thermodynamic calculations showed that the Fe/(Fe + Mg) ratios increase with decreasing fO_2 (Bryndzia and Scot, 1987a, b). Whole-rock compositions also control the Fe/(Fe + Mg) ratios of chlorite with positive correlation between them (Bevins et al., 1991; Xie et al., 1997). The host rock is homogeneous in our study, thus the increasing trend of Fe/(Fe + Mg) can be attributed to oxidation processes. In summary, the original ore-forming fluid was reduced and enriched in silicon and metal elements. After the precipitation of sulfide minerals, the upward migrating fluid was reduced and depleted in metal elements, which subsequently altered the surrounding granite. In the proximal end, the granite was intensely altered with high fluid/rock ratios, where chlorite mainly was in the form of veinlets along the fractures. Chlorite is mainly controlled by the fluid compositions with low Ti, Sc, Ga and V contents and formed under the reduced condition with high Fe/(Fe + Mg) ratios. In the distal end or the part lacking fractures, the granite was weakly altered with low fluid/rock ratios, chlorite inherited part of the compositions of biotite, showing higher Ti, Sc, Ga and V contents. When migrating upward, the fluid mixed with the oxidized meteoric fluid, which has been revealed by the H and O isotopes (Li et al., 2017), hence the chlorite have relative low Fe/(Fe + Mg) ratios.

6.4. Vertical chemical variations of chlorite in the drill hole and implications for exploration

Our chlorite chemical data show systematic vertical variations from weak to intense chloritization granites from the drill holes (Figs. 9, 10). With increasing chloritization intensity of granites, the MgO, TiO_2, Li, Zn, Sc, Ga, V and Co contents of chlorite decrease, while FeO, Sr, Th and Pb contents and Fe/(Fe + Mg) ratios increase. The compositional variations of chlorite are controlled by the composition of biotite, the compositions of fluids and the intensity of fluid-rock interaction during alteration. As hydrothermal fluid migrated through the pluton, strong fluid and rock interaction resulted in the intense chloritization, which made the veined chlorite enriched in Fe, Sr, Th and Pb, and depleted in HFSEs and transition elements. While, weak and moderate chloritization inherited the compositions of biotite to some extent. Generally, samples from the proximal end of the ore body show intense chloritization, and the distal samples show weak chloritization. Hence, this systematic chemical variation of chlorite could be used as an indicator of detecting the mineralization center of Ag-Au-Pb-Zn deposits.

Previous work on chlorite revealed compositional change from center to rim of porphyry deposits, e.g. Batu Hijau porphyry Cu deposit in Indonesia (Wilkinson et al., 2015) and Yangdong porphyry Cu deposit in NW China (Xiao et al., 2017). Wilkinson et al. (2015) found that Ti, V and Mg contents decrease with increasing distance from the porphyry hydrothermal center, whereas Fe, Li, Sr, Co and Zn contents increase. In Yangdong porphyry Cu deposit, Ti, Au, Sn decrease with increasing distance from the orebody, while Zn increases (Xiao et al., 2017). The variation trends of Li, Sr, Co, Zn of chlorite from the Niujuan ore deposit are consistent with previous work. However, opposite trends are observed in Ti, Mg, Fe, Sr and V between our data and the two porphyry Cu deposits (Wilkinson et al., 2015; Xiao et al., 2017). We suggest that this may be caused by the difference between the hydrothermal fluid composition and the host rock composition. Elements

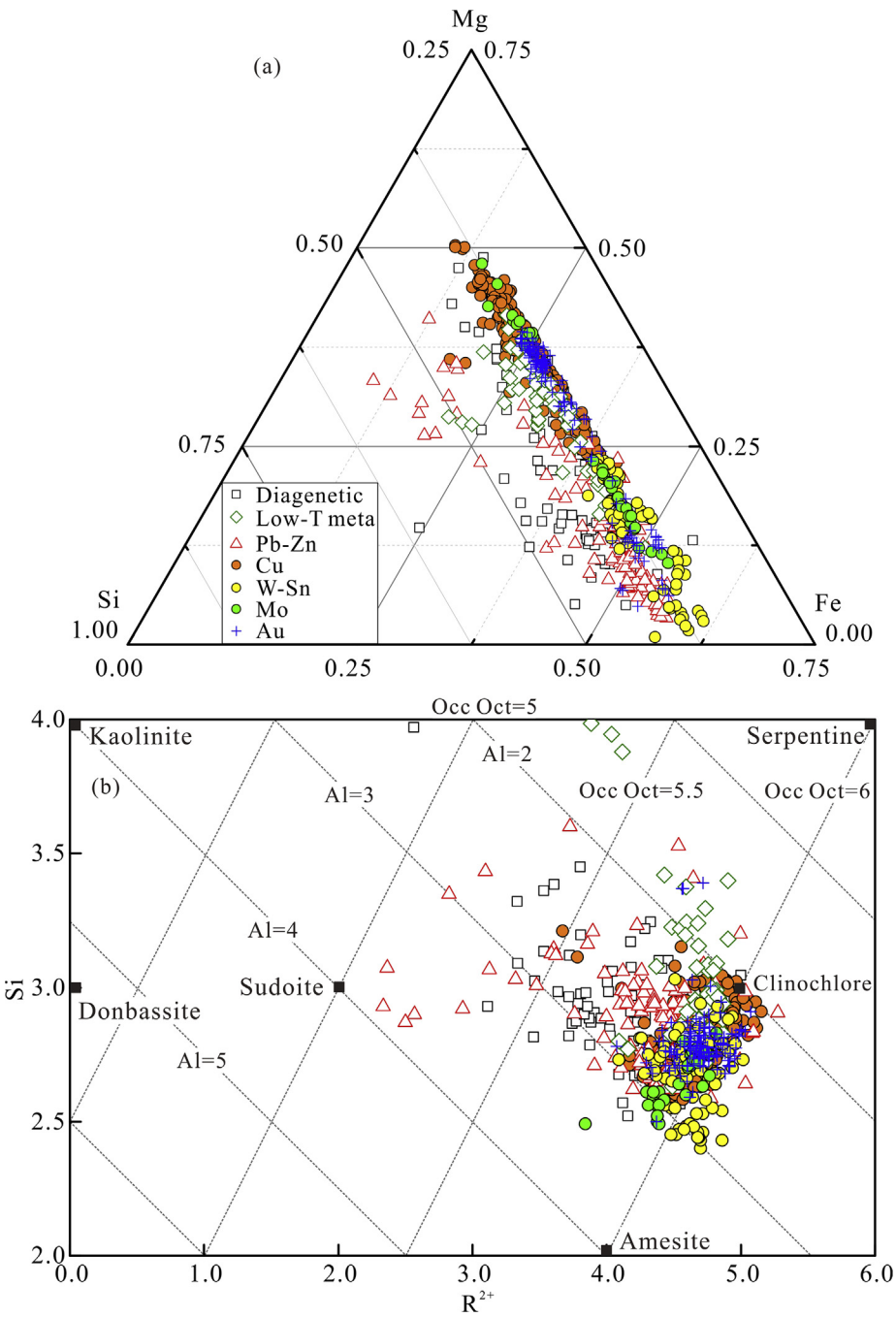

Fig. 14. Chemical variation of chlorite from different environments in terms of cations Si, Mg and Fe (a), and R^{2+} and Si (b, after Wiewiora and Weiss, 1990). Data of diagenetic chlorite are from Curtis (1985), Hillier and velde (1991), Hillier (1994), Jiang and Peacor (1994), Ryan and Reynolds (1997) and Barrenechea et al. (2000); Data of low-temperature metamorphic chlorite are from Bevins et al. (1991), Tulloch (1979) and Tarantola et al. (2009); Data of chlorite from the Cu deposits are from Melfos et al. (2002), Panigrahi et al. (2008), Li et al. (2012), Sun et al. (2015), Maydagán et al. (2016) and Xiao et al. (2017); Data of chlorite from the Pb-Zn deposits are from Ai and Liu (1998), Chinchilla et al. (2016), White et al. (2016) and this study; Data of chlorite from the Ag deposits are from Xiao et al. (1993), Zang and Fyfe (1995), Klein et al. (2007), Saravanan et al. (2009) and Zhang and Zhu (2016); Data of chlorite from the W-Sn deposits are from Zhao et al. (2005), Liao et al. (2010), Zhao et al. (2011) and Zhang et al. (2014); Data of chlorite from the Mo deposits are from Li (2011) and Ciesielczuk (2012).

brought in by the hydrothermal fluid will result in the high contents of these elements near the orebody. The composition of chlorite is controlled by the composition of the host rocks, in which Fe, Mg and Al were widely discussed by previous works (Zang and Fyfe, 1995; Xie et al., 1997; Lanari et al., 2014).

Overall, compositions of chlorite from different ore systems all show systematic variations, but with different trends. These studies suggest that (1) chlorite is a potential exploration tools both in high temperature porphyry Cu deposits and moderate-low temperature hydrothermal deposits; (2) different mineralization system have different compositional varieties of chlorite because of different compositions of host rocks and hydrothermal fluids. Therefore, we should build a criterion of composition varies of chlorite for the aimed mineralization system. We recommend paying more attention to the variations of fluid mobile elements, such as Sr, Th and Pb, and fluid immobile elements, such as HFSEs and transition elements.

6.5. Comparison with chlorite of different genesis

Chlorite is a common mineral found in a variety of geological environments including sedimentary, low-grade metamorphic and hydrothermally altered rocks (De Caritat, 1993). As shown in Fig. 14, chlorite from various geological environments has different compositions. Chlorite formed at low temperatures, such as diagenetic, low-temperature metamorphic environments and Pb-Zn deposits, has higher Si content than those formed at relatively high temperatures, such as Cu, Mo, W-Sn and Au deposits, which is probably related to the less Tschermark substitution ($Si + Fe \rightarrow Al^{IV} + Al^{VI}$) in chlorite at low temperatures (Cathelineau, 1988; Bourdelle et al., 2013). Less Al^{VI} is expected for the less Tschermark substitution. However, chlorite formed under low temperature conditions have higher Al^{VI} contents (low octahedral occupancy; Fig. 14b) than those formed at high temperatures, which indicates that, except for the Tschermark substitution,

the di-trioctahedral substitution $3(Mg^{2+}, Fe^{2+}) \rightarrow \square + 2Al^{VI}$ prevails at low temperatures. Compared with low temperature environments, chlorite from the hydrothermal deposits has low Al^{VI} contents (high octahedral occupancy), which is attributed to the di-trioctahedral substitution $\square + 2Al^{VI} \rightarrow 3(Mg^{2+}, Fe^{2+})$ for the generally high metallic elements in the ore-forming fluids. Substantial substitutions of Fe and Mg for Al reduce the octahedral vacancies in chlorite.

Chlorite from hydrothermal deposits has large variations of Fe and Mg contents and relatively uniform Si and Al contents. Chlorite from porphyry Cu deposits has high Mg and low Fe contents when compared with those from W-Sn deposits. The variations probably reflect the host-rock compositions, since the porphyry Cu deposits and the W-Sn deposits are genetically related with Mg-rich intermediate-felsic rocks and Mg-poor felsic rocks, respectively. This is consistent with the previous study that the chemical compositions of chlorite show good correlation with MgO of rock (e.g. Xie et al., 1997). Moreover, as an alteration mineral, chlorite usually occurs as an alteration mineral after primary igneous biotite and hornblende. The compositions of chlorite are influenced by the composition of these igneous minerals. The hornblende and biotite in intermediate-felsic rocks have higher MgO and lower FeO than the felsic rocks. The main data from Au deposits are concentrated in the relatively Mg-rich end-member, overlapping with those in porphyry Cu deposits (Fig. 14a), which suggest that Au deposits are more closely related with porphyry Cu deposits. As we discussed above, redox states could be another factor in controlling the Fe-Mg enrichment-depletion patterns. The W-Sn deposits and the Ag-Au-Pb-Zn deposit of this study with reduced systems develop Fe-rich chlorite, and the Cu deposits with oxidized system develop Mg-rich chlorite.

Mo deposits include Mo-dominated, W-Mo(-Sn-Bi) and Cu-Mo deposits (Zhong et al., 2017). Different types show different compositions in chlorite. The chlorite from the Mo deposits accompanied by Cu mineralization show Mg-rich features, while those from the Mo deposits accompanied with W-Sn mineralization are relatively Fe-rich.

7. Conclusions

(1) In the processes of chloritization of granite, evidences suggest that two biotite converted to one chlorite (2Bt → 1Chl) is the main alteration mechanism. Hydrothermal fluid mainly brought in Fe, Sr, Th, Pb and CO_2, and took out Mg, Ti, Si, F, K, Li, Zn, Sc, Ga, Co from the biotite during the alteration.
(2) Chlorite in quartz-chlorite veins was precipitated directly from the hydrothermal fluids. Veined chlorite in intensely altered granites formed by the dissolution-transport-precipitation mechanism. The hydrothermal fluids should have low fluid immobile elements, such as Ti, Ga, Sc and V and were reduced fluids.
(3) From weak to intense chloritization granites, FeO, Sr, Th and Pb contents increase, and MgO, TiO_2, Li, Zn, Sc, Ga, V, Co and Nb contents decrease. Compositional variations of chlorite are useful exploration tools of detecting moderate-low temperature deposits, such as the Niujuan Ag-Ag-Pb-Zn deposit.
(4) Compositions of chlorite from various geological environments mainly differ in Mg, Fe and Al^{IV}, which are mainly controlled by the compositions of host rocks and the formation temperature.

Acknowledgements

We are grateful to Fangyue Wang and Juan Wang for their assistance in LA-ICPMS and EMPA analyses, respectively, and to Jifan Sun for his assistance in sampling. We thank the editor and detailed reviews by John L Walshe and an anonymous reviewer, which led to significant improvement of the manuscript. This study is supported by National Natural Science Foundation of China (Grant Nos. 41602051, 41530206) and the Geological Survey of China (Grant No. 12120115033601).

Appendix A. Supplementary material

Supplementary data associated with this article can be found, in the online version, at https://doi.org/10.1016/j.oregeorev.2018.08.003.

References

Ai, Y.F., Liu, G.P., 1998. The study of chlorite at Dajing deposit in Inner-Mongolia of China. Acta Sci. Nat. Univ. Pek. 34, 99–107 (in Chinese with English abstract).
Bailey, S.W., 1988. Chlorites; structures and crystal chemistry. Rev. Mineral. Geochem. 19, 347–403.
Barrenechea, J.F., Rodas, M., Frey, M., Alonso-Azcárate, J., Mas, J.R., 2000. Chlorite, corrensite, and chlorite-mica in Late Jurassic fluvio-lacustrine sediments of the Cameros basin of northeastern Spain. Clay. Clay. Miner. 48, 256–265.
Beaufort, D., Rigault, C., Billon, S., Billault, V., Inoue, A., Inoue, S., Patrier, P., 2015. Chlorite and chloritization processes through mixed-layer mineral series in low-temperature geological systems – a review. Clay Minerals 50, 497–523.
Bevins, R.E., Robinson, D., Rowbotham, G., 1991. Compositional variations in mafic phyllosilicates from regional low-grade metabasites and application of the chlorite geothermometer. J. Metamorph. Geol. 9, 711–721.
Bourdelle, F., Parra, T., Beyssac, O., Chopin, C., Vidal, O., 2013. Clay minerals as geothermometer: a comparative study based on high spatial resolution analyses of illite and chlorite in Gulf Coast sandstones (Texas, USA). Am. Mineral. 98, 914–926.
Bryndzia, L.T., Scott, S.D., 1987a. The composition of chlorite as a function of sulfur and oxygen fugacity; an experimental study. Am. J. Sci. 287, 50–76.
Bryndzia, L.T., Scott, S.D., 1987b. Application of chlorite-sulphide-oxide equilibria to metamorphosed sulphide ores, Snow Lake area. Manitoba. Econ. Geol. 82, 963–970.
Brzozowski, M.J., Samson, I.M., Gagnon, J.E., Linnen, R.L., Good, D.J., Ames, D.E., Flemming, R., 2018. Controls on the chemistry of minerals in late-stage veins and implications for exploration vectoring tools for mineral deposits: an example from the Marathon Cu-Pd deposit, Ontario, Canada. J. Geochem. Explor. 190, 109–129.
Cathelineau, M., 1988. Cation site occupancy in chlorites and illites as function of temperature. Clay Miner. 23, 471–485.
Cathelineau, M., Nieva, D., 1985. A chlorite solid solution geothermometer the Los Azufres (Mexico) geothermal system. Contrib. Mineral. Petr. 91, 235–244.
Chang, Z., Hedenquist, J.W., White, N.C., Cooke, D.R., Roach, M., Deyell, C.L., Garcia, J., Gemmell, J.B., McKnight, S., Cuison, A.L., 2011. Exploration tools for linked porphyry and epithermal deposits: example from the mankayan intrusion-centered Cu-Au district, Luzon, Philippines. Econ. Geol. 106, 1365–1398.
Chayes, F., 1955. Potash feldspar as a by-product of the biotite-chlorite transformation. J. Geol. 63, 75–82.
Chen, W.J., Liu, H.T., Zhang, D.H., 2007. Fluid inclusion's characteristics of the Niujuan silver deposit in Fengning, Hebei, and its geological significance. Miner. Resour. Geol. 21, 12–16 (in Chinese with English abstract).
Chinchilla, D., Arroyo, X., Merinero, R., Piña, R., Nieto, F., Ortega, L., Lunar, R., 2016. Chlorite geothermometry applied to massive and oscillatory-zoned radiated Mn-rich chlorites in the Patricia Zn-Pb-Ag epithermal deposit (NE, Chile). Appl. Clay Sci. 134 (Part 3), 210–220.
Ciesielczuk, J., 2012. Chlorite of hydrothermal origin in the Strzelin and Borów granites (Fore-Sudetic Block, Poland). Geol. Q. 56, 333–344.
Cook, N.J., Ciobanu, C.L., Pring, A., Skinner, W., Shimizu, M., Danyushevsky, L., Saini-Eidukat, B., Melcher, F., 2009. Trace and minor elements in sphalerite: a LA-ICPMS study. Geochim. Cosmochim. Acta 73, 4761–4791.
Curtis, C.D., 1985. Compositional variation within some sedimentary chlorites and some comments on their origin. Mineral. Mag. 49, 375–386.
Davis, G.A., Cong, W., Yadong, Z., Jinjiang, Z., Changhou, Z., Gehrels, G.E., 1998. The enigmatic Yinshan fold-and-thrust belt of northern China: new views on its intraplate contractional styles. Geology 26, 43–46.
De Caritat, P., 1993. Chlorite geothermometry: a review. Clay. Clay Miner. 41, 219–239.
Eggleton, R.A., Banfield, J.F., 1985. The alteration of granitic biotite to chlorite. Am. Mineral. 70, 902–910.
Ferry, J.M., 1979. Reaction mechanisms, physical conditions, and mass transfer during hydrothermal alteration of mica and feldspar in granitic rocks from south-central Maine, USA. Contrib. Mineral. Petr. 68, 125–139.
Foster M.D., 1962. Interpretation of the composition and a classification of the chlorites.
Griffin, W., Andi, Z., O'reilly, S., Ryan, C., 1998. Phanerozoic evolution of the lithosphere beneath the Sino-Korean craton. Mantle dynamics and plate interactions in East Asia, pp. 107–126.
Halter, W.E., Williams-Jones, A.E., Kontak, D.J., 1998. Modeling fluid–rock interaction during greisenization at the East Kemptville tin deposit: implications for mineralization. Chem. Geol. 150, 1–17.
Hart, C.J., Goldfarb, R.J., Qiu, Y., Snee, L., Miller, L.D., Miller, M.L., 2002. Gold deposits of the northern margin of the North China Craton: multiple late Paleozoic-Mesozoic mineralizing events. Miner. Deposita 37, 326–351.
Hayes, J.B., 1970. Polytypism of chlorite in sedimentary rocks. Clay. Clay Miner. 18, 285–306.
Hillier, S., 1994. Pore-lining chlorites in siliciclastic reservoir sandstones; electron microprobe, SEM and XRD data, and implications for their origin. Clay Miner. 29, 665–679.
Hillier, S., Velde, B., 1991. Octahedral occupancy and chemical composition of diagenetic (low-temperature) chlorites. Clay Miner. 26, 149–168.
Inoue, A., Kurokawa, K., Hatta, T., 2010. Application of chlorite geothermometry to hydrothermal alteration in Toyoha geothermal system, Southwestern Hokkaido, Japan. Resour. Geol. 60, 52–70.
Inoue, A., Meunier, A., Patriermas, P., Rigault, C., Beaufort, D., Vieillard, P., 2009. Application of chemical geothermometry to low-temperature trioctahedral chlorites. Clay. Clay Miner. 57, 371–382.
Jahren, J., Aagaard, P., 1989. Compositional variations in diagenetic chlorites and illites,

and relationships with formation-water chemistry. Clay Miner. 24, 157–170.
Jiang, W.T., Peacor, D.R., 1994. Formation of corrensite, chlorite and chlorite-mica stacks by replacement of detrital biotite in low-grade pelitic rocks. J. Metamorph. Geol. 12, 867–884.
Jowett, E., 1991. Fitting iron and magnesium into the hydrothermal chlorite geothermometer. GAC/SEG Joint Annual Meeting, Toronto, Program with Abstracts. p. A62.
Klein, E.L., Harris, C., Giret, A., Moura, C.A.V., 2007. The Cipoeiro gold deposit, Gurupi Belt, Brazil: geology, chlorite geochemistry, and stable isotope study. J. S. Am. Earth Sci. 23, 242–255.
Kranidiotis, P., MacLean, W., 1987. Systematics of chlorite alteration at the Phelps Dodge massive sulfide deposit, Matagami, Quebec. Econ. Geol. 82, 1898–1911.
Lanari, P., Wagner, T., Vidal, O., 2014. A thermodynamic model for di-trioctahedral chlorite from experimental and natural data in the system MgO–FeO–Al2O3–SiO2–H2O: applications to P-T sections and geothermometry. Contrib. Mineral. Petr. 167, 968.
Li, J., Li, G., Qin, K., Xiao, B., Chen, L., Zhao, J., 2012. Mineralogy and mineral chemistry of the cretaceous duolong gold-rich porphyry copper deposit in the bangongco arc, Northern Tibet. Resour. Geol. 62, 19–41.
Li, L., 2011. Study of characters of biotite and chlorite of molybdenum deposit in Antuoling, Hebei. Master's Dissertation, China University of Geosciences (Beijing) (in Chinese with English abstract).
Li, Y.G., Wang, L.X., 2002. The study on wall rock alteration of Niujuan silver (gold) deposit, Hebei Province, China. Contrib. Geol. Miner. Resour. Res. 17, 234–239 (in Chinese with English abstract).
Li, Y.J., Li, S.R., Santosh, M., Mo, X.X., Gao, K.B., Ma, Y., 2017. Isotope geochemistry and geochronology of the Niujuan silver deposit, northern North China Craton: Implications for magmatism and metallogeny in an extensional tectonic setting. Ore Geol. Rev. 90, 36–51.
Liao, Z., Liu, Y.P., Li, C.Y., Ye, S., Liu, S.R., Zheng, W.Q., 2010. Characteristics of chlorites from Dulong Sn-Zn deposit and their metallogenic implications. Miner. Deposits 29, 169–176 (in Chinese with English abstract).
Liu, Y., Hu, Z., Gao, S., Günther, D., Xu, J., Gao, C., Chen, H., 2008. In situ analysis of major and trace elements of anhydrous minerals by LA-ICP-MS without applying an internal standard. Chem. Geol. 257, 34–43.
Lowell, J.D., Guilbert, J.M., 1970. Lateral and vertical alteration-mineralization zoning in porphyry ore deposits. Econ. Geol. 65, 373–408.
Martinez-Serrano, R.G., Dubois, M., 1998. Chemical variations in chlorite at the Los Humeros geothermal system, Mexico. Clay. Clay Miner. 46, 615–628.
Maydagán, L., Franchini, M., Impiccini, A., Lentz, D., 2016. Phyllosilicates geochemistry and distribution in the Altar porphyry Cu-(Au) deposit, Andes Cordillera of San Juan, Argentina: applications in exploration, geothermometry, and geometallurgy. J. Geochem. Explor. 167, 83–109.
Maydagán, L., Franchini, M., Impiccini, A., Lentz, D., Patrier, P., Beaufort, D., 2018. Chlorite, white mica and clay minerals as proximity indicators to ore in the shallow porphyry environment of Quebrada de la Mina deposit, Argentina. Ore Geol. Rev. 92, 297–317.
McDowell, S.D., Elders, W.A., 1980. Authigenic layer silicate minerals in borehole Elmore 1, Salton Sea geothermal field, California, USA. Contrib. Mineral. Petr. 74, 293–310.
Melfos, V., Vavelidis, M., Christofides, G., Seidel, E., 2002. Origin and evolution of the Tertiary Maronia porphyry copper-molybdenum deposit, Thrace, Greece. Miner. Deposita 37, 648–668.
Miller, L., Goldfarb, R., Nie, F., Hart, C., Miller, M., Yang, Y., Liu, Y., 1998. North China gold: a product of multiple orogens. Soc. Econ. Geol. Newslett. 33, 1–12.
Morad, S., El-Ghali, M.A., Caja, M.A., Al-Ramadan, K., Mansurbeg, H., 2009. Hydrothermal alteration of magmatic titanite: evidence from Proterozoic granitic rocks, southeastern Sweden. Can. Mineral. 47, 801–811.
Nie, F.J., Zhang, W.Y., Jiang, S.H., Liu, Y., 2007. Discussion on the time limitation of silver (gold) mineralization in the Niujuan deposit, Northern Hebei Province. Earth Sci. Front. 14, 167–176 (in Chinese with English abstract).
Panigrahi, Mruganka K., Naik, Rajesh K., Pandit, D., Misra, Kula C., 2008. Reconstructing physico-chemical parameters of hydrothermal mineralization of copper at the Malanjkhand deposit, India, from mineral chemistry of biotite, chlorite and epidote. Geochem. J. 42, 443–460.
Papoulis, D., Tsolis-Katagas, P., Kalampounias, A.G., Tsikouras, B., 2009. Progressive formation of halloysite from the hydrothermal alteration of biotite and the formation mechanisms of rutile in altered volcanic rocks from Limnos Island, northeast Aegean Sea, Greece. Clay. Clay Miner. 57, 566–577.
Parneix, J.C., Beaufort, D., Dudoignon, P., Meunier, A., 1985. Biotite chloritization process in hydrothermally altered granites. Chem. Geol. 51, 89–101.
Rieder, M., Cavazzini, G., D'Yakonov, Y.S., Frank-Kamenetskii, V.A., Gottardi, G., Guggenheim, S., Koval, P.V., Muller, G., Neiva, A.M.R., Radoslovich, E.W., Robert, J.L., Sassi, F.P., Takeda, H., Weiss, Z., Wones, D.R., 1998. Nomenclature of the micas. Can. Mineral. 36, 905–912.
Ryan, P.C., Reynolds, R.C., 1996. The origin and diagenesis of grain-coating serpentine-chlorite in Tuscaloosa Formation sandstones, U.S. Gulf Coast. Am. Mineral. 81, 213–225.
Ryan, P.C., Reynolds, R.C., 1997. The chemical composition of serpentine/chlorite in the Tuscaloosa Formation, United States Gulf Coast; EDX vs. XRD determinations, implications for mineralogic reactions and the origin of rutile. Clay. Clay Miner. 45, 339–352.
Saravanan, C.S., Mishra, B., Jairam, M.S., 2009. P-T conditions of mineralization in the Jonnagiri granitoid-hosted gold deposit, eastern Dharwar Craton, southern India: constraints from fluid inclusions and chlorite thermometry. Ore Geol. Rev. 36, 333–349.
Shen, L.X., Li, W.S., Wang, Z.L., Ding, J.D., Ma, J.X., Li, X.Y., 2012. Forecast for the deep mineralization of Niujuan silver-gold deposit and Yingfang silver-lead-zinc deposit in northern Hebei Province. Contrib. Geol. Miner. Resour. Res. 27, 450–457 (in Chinese with English abstract).
Shriver, N., MacLean, W., 1993. Mass, volume and chemical changes in the alteration zone at the Norbec mine, Noranda, Quebec. Miner. Deposita 28, 157–166.
Sun, J.G., Li, H.Y., Liu, X.H., Xie, K.Q., Chen, W., Xue, D.S., Sun, X.L., 2015. Characteristics of chlorite from the Tongkuangyu copper deposit in Shanxi Province and their geological implications. Bull. Mineral. Petrol. Geochem. 34, 1142–1154 (in Chinese with English abstract).
Tarantola, A., Mullis, J., Guillaume, D., Dubessy, J., de Capitani, C., Abdelmoula, M., 2009. Oxidation of CH4 to CO2 and H2O by chloritization of detrital biotite at 270 ± 5 °C in the external part of the Central Alps, Switzerland. Lithos 112, 497–510.
Tulloch, A.J., 1979. Secondary Ca-Al silicates as low-grade alteration products of granitoid biotite. Contrib. Mineral. Petr. 69, 105–117.
Veblen, D.R., Ferry, J.M., 1983. A TEM study of the biotite-chlorite reaction and comparison with petrologic observations. Am. Mineral. 68, 1160–1168.
Vidal, O., De Andrade, V., Lewin, E., Munoz, M., Parra, T., Pascarelli, S., 2006. P-T-deformation-Fe3+/Fe2+ mapping at the thin section scale and comparison with XANES mapping: application to a garnet-bearing metapelite from the Sambagawa metamorphic belt (Japan). J. Metamorph. Geol. 24, 669–683.
Vidal, O., Parra, T., 2000. Exhumation paths of high-pressure metapelites obtained from local equilibria for chlorite–phengite assemblages. Geol. J. 35, 139–161.
Vidal, O., Parra, T., Trotet, F., 2001. A thermodynamic model for Fe-Mg aluminous chlorite using data from phase equilibrium experiments and natural pelitic assemblages in the 100° to 600°c, 1 to 25 kb Range. Am. J. Sci. 301, 557–592.
Walker, J.R., 1993. Chlorite polytype geothermometry. Clay. Clay. Miner. 41, 260–267.
Walshe, J.L., 1986. A six-component chlorite solid solution model and the conditions of chlorite formation in hydrothermal and geothermal systems. Econ. Geol. 81, 681–703.
Wei, X.Y., 2000. Discussion on structural control characteristics and genesis of Yingfang-Niujuan silver deposit, Hebei. Contrib. Geol. Miner. Resour. Res. 15 261-266+281 (in Chinese with English abstract).
White, A.J.R., Pearce, M.A., Meadows, H.R., 2016. Distinguishing regional- and local-scale metasomatic systems at the Prairie Downs Zn–Pb deposit. Lithos 262, 247–265.
Wiewiora, A., Weiss, Z., 1990. Crystallochemical classifications of phyllosilicates based on the unified system of projection of chemical composition; II, The chlorite group. Clay Minerals 25, 83–92.
Wilkinson, J.J., Chang, Z., Cooke, D.R., Baker, M.J., Wilkinson, C.C., Inglis, S., Chen, H., Bruce, Gemmell J., 2015. The chlorite proximitor: a new tool for detecting porphyry ore deposits. J. Geochem. Explor. 152, 10–26.
Xiao, B., Chen, H., Wang, Y., Han, J., Xu, C., Yang, J., 2017. Chlorite and epidote chemistry of the Yandong Cu deposit, NW China: Metallogenic and exploration implications for Paleozoic porphyry Cu systems in the Eastern Tianshan. Ore Geol. Rev. In Press.
Xiao, Z.F., Ouyang, Z.Y., Lu, H.Z., Cheng, J.P., 1993. The characteristics of chlorites in the wall-rock alteration zone in the Baoban gold field, Hainan island with emphasis on the physico-chemical conditions of hydrothermal alteration. Acta Mineral. Sin. 14, 319–324 (in Chinese with English abstract).
Xie, X., Byerly, G.R., Ferrell Jr., R.E., 1997. IIb trioctahedral chlorite from the Barberton greenstone belt: crystal structure and rock composition constraints with implications to geothermometry. Contrib. Mineral. Petr. 126, 275–291.
Yang, J.H., Wu, F.Y., Wilde, S.A., 2003. A review of the geodynamic setting of large-scale Late Mesozoic gold mineralization in the North China Craton: an association with lithospheric thinning. Ore Geol. Rev. 23, 125–152.
Yavuz, F., Kumral, M., Karakaya, N., Karakaya, M.Ç., Yıldırım, D.K., 2015. A Windows program for chlorite calculation and classification. Comput. Geosci. 81, 101–113.
Yuguchi, T., Sasao, E., Ishibashi, M., Nishiyama, T., 2015. Hydrothermal chloritization processes from biotite in the Toki granite, Central Japan: temporal variations of the compositions of hydrothermal fluids associated with chloritization. Am. Mineral. 100, 1134–1152.
Zane, A., Weiss, Z., 1998. A procedure for classifying rock-forming chlorites based on microprobe data. Rend. Lincei 9, 51–56.
Zang, W., Fyfe, W.S., 1995. Chloritization of the hydrothermally altered bedrock at the Igarapé Bahia gold deposit, Carajás, Brazil. Miner. Deposita 30, 30–38.
Zhang, H., Zhu, Y., 2016. Geology and geochemistry of the Huilvshan gold deposit, Xinjiang, China: implications for mechanism of gold precipitation. Ore Geol. Rev. 79, 218–240.
Zhang, S.H., Zhao, Y., 2013. Mid-crustal emplacement and deformation of plutons in an Andean-style continental arc along the northern margin of the North China Block and tectonic implications. Tectonophysics 608, 176–195.
Zhang, S.H., Zhao, Y., Liu, X.C., Liu, D.Y., Chen, F., Xie, L.W., Chen, H.-H., 2009. Late Paleozoic to Early Mesozoic mafic–ultramafic complexes from the northern North China Block: constraints on the composition and evolution of the lithospheric mantle. Lithos 110, 229–246.
Zhang, W., Zhang, S.T., Cao, W.H., Wu, J.D., Xiao, C.X., Cheng, H.J., Tang, L., 2014. Characteristics of chlorite minerals from Xiaolonghe tin deposit in West Yunnan, China and their geological implications. J. Chengdu Univ. Tech. (Sci. Tech. Edition) 41, 318–328 (in Chinese with English abstract).
Zhao, K.D., Jiang, S.Y., Jiang, Y.H., Wang, R.C., 2005. Mineral chemistry of the Qitianling granitoid and the Furong tin oredeposit in Hunan Province, South China: implication for the genesis of granite and related tin mineralization. Eur. J. Mineral. 17, 635–648.
Zhao, Z.J., Lu, J.J., Yao, Y., Zhang, R.Q., Guo, W.M., Zhang, H.F., Xie, X., 2011. Chloritization of Qitianling granite related to Bailashui tin deposit, southern Hunan Province. Geol. J. China Univ. 17, 531–545 (in Chinese with English abstract).
Zhong, J., Chen, Y.J., Pirajno, F., 2017. Geology, geochemistry and tectonic settings of the molybdenum deposits in South China: a review. Ore Geol. Rev. 81 (Part 2), 829–855.